

# Hyper Ramsey-Bordé matter-wave interferometry for robust quantum sensors

T. Zanon-Willette,<sup>1,2,3</sup> D. Wilkowski,<sup>2,3,4</sup> A.V. Taichenachev,<sup>5,6</sup> and V.I. Yudin<sup>5,6,7</sup>

<sup>1</sup>*Sorbonne Université, Observatoire de Paris, Université PSL, CNRS, LERMA, F-75005, Paris, France\**

<sup>2</sup>*MajuLab, CNRS-UCA-SU-NUS-NTU International Joint Research Unit, Singapore,*

<sup>3</sup>*Centre for Quantum Technologies, National University of Singapore, 117543 Singapore, Singapore.*

<sup>4</sup>*School of Physical and Mathematical Sciences, Nanyang Technological University, 637371 Singapore, Singapore.*

<sup>5</sup>*Novosibirsk State University, ul. Pirogova 2, 630090 Novosibirsk, Russia*

<sup>6</sup>*Institute of Laser Physics, Siberian Branch, Russian Academy of Sciences, prosp. Akad. Lavrent'eva 15B, 630090 Novosibirsk, Russia*

<sup>7</sup>*Novosibirsk State Technical University, prosp. Karla Marksa 20, 630073 Novosibirsk, Russia*

(Dated: April 21, 2021)

A new generation of atomic sensors using ultra-narrow optical clock transitions and composite pulses are pushing quantum engineering control to a very high level of precision for applied and fundamental physics. Here, we propose a new version of Ramsey-Bordé interferometry introducing arbitrary composite laser pulses with tailored pulse duration, Rabi field, detuning and phase-steps. We explore quantum metrology below the  $10^{-18}$  level of fractional accuracy by a fine tuning control of light excitation parameters protecting ultra-narrow optical clock transitions against residual light-shift coupled to laser-probe field variation. We present, for the first time, new developments for robust hyper Ramsey-Bordé and Mach-Zehnder interferometers, where we protect wavepacket interferences against distortion on frequency or phase measurement related to residual Doppler effects and light-shifts coupled to a pulse area error. Quantum matter-wave sensors with composite pulses and ultra-cold sources will offer detection of inertial effects inducing phase-shifts with better accuracy, to generate hyper-robust optical clocks and improving tests of fundamental physics, to realize a new class of atomic interferometers tracking space-time gravitational waves with a very high sensitivity.

## I. INTRODUCTION

Seventy years ago, Ramsey established the first quantum mechanical description of an interferometric resonance with the method of separated oscillating fields [1]. Ramsey spectroscopy with coherent radiation and phase manipulation became a very effective tool to investigate internal properties of nuclei, atoms and molecules [2–4] while opening a revolution in quantum metrology with atomic fountains as primary frequency standards reaching today a fractional frequency accuracy of  $2 \times 10^{-16}$  [5].

By labeling internal states with momentum quantization, Bordé has extended the method of separated oscillating field to atomic interferometry with optical transitions realizing laser beam splitters and mirrors for matter-waves [6–8]. Pioneering works on interferences with atoms were also made by Chebotayev and Dubetsky based on separated optical fields with standing waves [9, 10]. Ramsey-Bordé interferometers using cold and ultra-cold atom techniques have reached high sensitivity to rotation [11, 12], acceleration [13], accurate determination of the fine structure constant [14–19] or optical clock realization with supersonic beams reaching a fractional frequency instability around  $2 \times 10^{-16}$  [20]. Mach-Zehnder type quantum sensors have thus been developed for gravitational field measurements [21–23].

In parallel to laser spectroscopy and atom interferometry, composite pulses in Nuclear Magnetic Resonance (NMR) became a powerful tool to compensate for several imperfections due to radio-frequency (rf) pulses applied on large samples of nuclear spins [24, 25]. Various signal distortions from rf field inhomogeneities, off-resonance effects and field amplitude error were reduced to a very low order of correction by means of complex sequences of pulses adapted to single or even dual compensation of these systematics. Composite pulses have also demonstrated to be useful for robust error compensation in high-fidelity qubit gates dedicated to quantum computation [26–28].

So far, understanding how to improve the robustness of precision measurements while reducing laser-probe-induced systematics still remains a critical goal for quantum sensing. But contrary to recent composite NMR-like pulse techniques applied in interferometers [29–31], composite laser pulses are required to reduce or eliminate residual phase-shifts leading to distortions of interferometric resonances. A major step in that direction was realized in 2010 with the introduction of the hyper-Ramsey scheme to experimentally reduce laser-probe induced frequency shifts by several orders of magnitude in optical clocks requiring large probe intensities [32, 33]. A sequence of two Ramsey pulses was used where an additional third one acts like a spin echo compensation of field amplitude error. This extra pulse can be inserted either before or after the free evolution time to strongly reduce the residual phase-shift [34]. Moreover, new generalized hyper-Ramsey protocols have extended robustness of probing clock transitions against residual light-shifts

\* thomas.zanon@sorbonne-universite.fr

coupled to decoherence [35, 36].

The main motivation of this work is to bring optical composite pulses to matter-wave interferometry with efficient nonlinear compensation of pulse-defects induced phase-shifts while these methods are usually absent in modern atomic interferometry [37–39]. We will revisit Ramsey-Bordé interferometry including internal state labeling, light-shift, Doppler-shift and atomic recoil with arbitrary sequences of composite pulses around a single free evolution time. A universal building-block with two-level operators, shown in Fig.1, is developed through **section II**, offering an efficient computational algorithm to explore interferometric resonances and phase-shifts produced by composite pulses dragging matter-waves. Small variations in laser pulses parameters are compensated by generating sophisticated path trajectories on a Bloch's sphere reducing any distortion of matter-wave components over the entire pulse interrogation protocol. We will review a few robust composite pulse schemes for hyper-clocks in **section III**. Beside well-known results on clock interferometry with multi-pulses, this section goal is to validate our computational method of elementary building-block decomposition when concatenated pulses are interleaved with several free evolution times. In **section IV**, we extend the method of composite pulses to hyper interferometers with matter-waves which act against laser pulse errors induced by laser intensity variation during interrogation protocols. We conclude about the potential impact of applying composite pulses with laser phase-step protocols in Ramsey-Bordé matter-wave interferometry within **section V**.

## II. HYPER RAMSEY-BORDÉ BUILDING-BLOCK

We present here a universal framework relying on concepts of hyper-Ramsey probing schemes for clock interferometry using two-level operators that simplify the description of matter-waves propagating through several optical composite pulses. One can address first a large variety of multiple probe excitation pulses inducing technical shifts and defects that are leading to significant measurement errors in a conventional atomic interferometer. Then our algorithm allows to explore clusters of multi-composite pulses interleaved with several free evolution times that may provide a better compensation of errors in laser parameters perturbing the matter-wave amplitude probability.

The formal derivation of the generalized Ramsey-Bordé amplitude probability  $\Psi(t)$  is based on Cayley-Klein parametrization of rotation spinors as [40]:

$$M(\tilde{\vartheta}_l) = \begin{pmatrix} \cos \tilde{\vartheta}_l e^{i\phi_l} & -ie^{-i(\varphi_l)} \sin \tilde{\vartheta}_l \\ -ie^{i(\varphi_l)} \sin \tilde{\vartheta}_l & \cos \tilde{\vartheta}_l e^{-i\phi_l} \end{pmatrix}, \quad (1)$$

with the action of a phase  $\varphi_l$  on the Rabi complex fre-

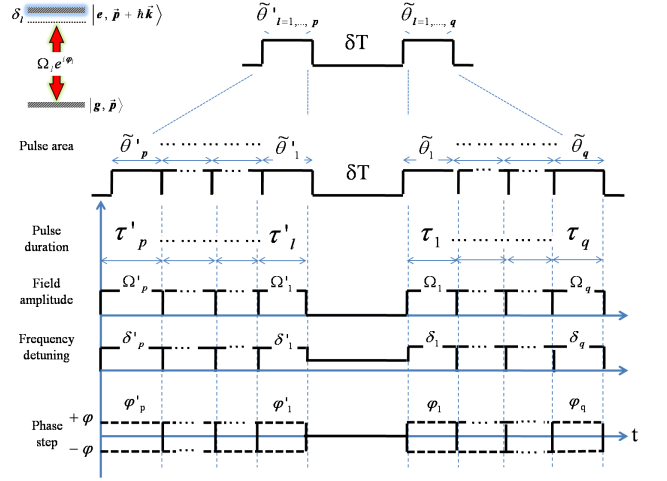


FIG. 1. (color online). Universal hyper-Ramsey-Bordé building-block denoted as  ${}^qM(\uparrow)(\downarrow)$  for composite pulse matter-wave interferometry with optical traveling waves. Arbitrary composite pulses are introduced by pulse area  $\tilde{\vartheta}'_{l=1,\dots,p}$  and  $\tilde{\vartheta}_{l=1,\dots,q}$  around a single Ramsey free evolution time  $T$ . Pulse parameters are phases  $\varphi'_l, \varphi_l$ , fields excitation  $\Omega'_l, \Omega_l$ , pulses duration  $\tau'_l, \tau_l$  and frequency detunings  $\delta'_l, \delta_l$  including transverse Doppler-shifts  $k v_z$  related to arrow orientation  $\uparrow, \downarrow$ , atomic recoil  $\delta_r$  and a compensation of a potential residual light-shift  $\Delta'_l, \Delta_l$ .

quency  $\Omega_l$ . Phase angles are introduced by:

$$\tilde{\vartheta}_l = \arcsin \left[ \frac{\Omega_l}{\omega_l} \sin \tilde{\theta}_l \right], \quad (2a)$$

$$\phi_l = \arctan \left[ \frac{\delta_l}{\omega_l} \tan \tilde{\theta}_l \right]. \quad (2b)$$

The effective pulse area is  $\tilde{\theta}_l = \theta_l/2 = \omega_l \tau_l/2$  with a generalized Rabi frequency denoted as  $\omega_l = \sqrt{\delta_l^2 + \Omega_l^2}$ . The effective detuning  $\delta_l = \delta + \Delta_l$  is a free detuning  $\delta$  including Doppler-shift and quantized atomic recoil when required as in [41] with the residual uncompensated part of the light-shift  $\Delta_l$ . Such a parametrization is emphasizing the role of any residual light-shift correction as an additional phase factor acting on diagonal elements of the interaction matrix.

Our model is based on the exact description of a full composite wave-function with spinors [40–42] incorporating independent control and fine tuning of coherent radiation parameters in the following form:

$$\Psi(t) = \left[ \overleftarrow{\prod}_{l=1}^q M(\tilde{\vartheta}_l) \right] \cdot M(\delta T) \cdot \left[ \overrightarrow{\prod}_{l=1}^p M(\tilde{\vartheta}'_l) \right] \Psi(0), \quad (3)$$

Each arrow indicates the direction to develop the product of matrices around a single free evolution time matrix  $M(\delta T)$  where laser fields, thus the light-shifts, are switch-off.

Complex amplitudes of  $\Psi(t)$  for a two-level spin system being initially prepared in  $\Psi(t=0)$ , can be obtained by

the application of successive  $p$  pulses before and  $q$  pulses after the free evolution time (See Fig. 1) leading to a complex matrix given by [44]:

$$\Psi(t) = {}^q_p M \cdot \Psi(0) \quad (4a)$$

$$\begin{pmatrix} C_g(t) \\ C_e(t) \end{pmatrix} = \begin{pmatrix} {}^q_p C_{gg} & {}^q_p C_{ge} \\ {}^q_p C_{eg} & {}^q_p C_{ee} \end{pmatrix} \cdot \begin{pmatrix} C_g(0) \\ C_e(0) \end{pmatrix}. \quad (4b)$$

where  ${}^q_p M$  is a special unitary operator and relations between the matter-wave components are  ${}^q_p C_{gg} = {}^q_p C_{ee}^*$ ,  ${}^q_p C_{ge} = -{}^q_p C_{eg}^*$ ,  $|{}^q_p C_{gg}|^2 + |{}^q_p C_{ge}|^2 = 1$ .

The complex probability amplitude associated to  ${}^q_p C_{gg}$  and  ${}^q_p C_{ge}$  can be recast into a symmetric canonical form as following:

$${}^q_p C_{gg} = {}^q_p \alpha_{gg} e^{i\delta T/2} \left[ 1 - |{}^q_p \beta_{gg}| e^{-i(\delta T + {}^q_p \Phi_{gg})} \right], \quad (5a)$$

$${}^q_p C_{ge} = {}^q_p \alpha_{ge} e^{i\delta T/2} \left[ 1 + |{}^q_p \beta_{ge}| e^{-i(\delta T + {}^q_p \Phi_{ge})} \right], \quad (5b)$$

Remarkably, we have found that complex parameters  $\alpha$  and  $\beta$  driving the overall envelop and composite phase-shifts can be also separated in two independent contributions from  $p$  pulses driven by pulse area  $\tilde{\vartheta}'_l$  and  $q$  pulses driven by  $\tilde{\vartheta}_l$  as following:

$${}^q_p \alpha_{gg} = \alpha_l'^p(gg) \cdot \alpha_l^q(gg), \quad (6a)$$

$${}^q_p \beta_{gg} = \beta_l'^p(gg) \cdot \beta_l^q(gg), \quad (6b)$$

$${}^q_p \alpha_{ge} = \alpha_l'^p(ge) \cdot \alpha_l^q(ge), \quad (6c)$$

$${}^q_p \beta_{ge} = \beta_l'^p(ge) \cdot \beta_l^q(ge). \quad (6d)$$

Envelop terms  ${}^q_p \alpha_{gg}$  and  ${}^q_p \alpha_{ge}$  have been explicitly developed for arbitrary cases in the appendix section S0 following [45]. From Eq. 5a and Eq. 5b, it follows that interferometric phase-shifts affecting the central interference  ${}^q_p \Phi_{gg}$  or  ${}^q_p \Phi_{ge}$  are given by:

$${}^q_p \Phi_{gg} = \varphi_L + \phi_L - (\text{Arg}[\beta_l'^p(gg)] + \text{Arg}[\beta_l^q(gg)]), \quad (7a)$$

$${}^q_p \Phi_{ge} = \varphi_L + \phi_L - (\text{Arg}[\beta_l'^p(ge)] + \text{Arg}[\beta_l^q(ge)]), \quad (7b)$$

with a remnant phase definition  $\varphi_L = \varphi_1 - \varphi'_1$  corrected by a light-shifted contribution  $\phi_L = \phi'_1 + \phi_1$  from pulses forming the original two-pulse Ramsey configuration. Note that phase-factors are now including a contribution from an arbitrary number of optical composite pulses extending previous results with three pulses [40].

Let's now derive the formal expression of complex factors  $\beta_l'^p(gg)$  and  $\beta_l^q(gg)$  leading to a main distortion of matter-waves interferences. Composites phase-shifts  ${}^q_p \Phi_{gg}$  and  ${}^q_p \Phi_{ge}$  are driven by a truncated continued frac-

tion expansion with  $p, q$  pulses as following:

$$\beta_l'^p(gg) = \frac{\tan \tilde{\vartheta}'_1 + e^{-i\Xi'_{12}} \frac{\tan \tilde{\vartheta}'_2 + e^{-i\Xi'_{23}} \frac{\tan \tilde{\vartheta}'_3 + \dots}{1-\dots}}{1 - e^{-i\Xi'_{23}} \tan \tilde{\vartheta}'_2 \frac{\tan \tilde{\vartheta}'_3 + \dots}{1-\dots}}}{1 - e^{-i\Xi'_{12}} \tan \tilde{\vartheta}'_1 \frac{\tan \tilde{\vartheta}'_2 + e^{-i\Xi'_{23}} \frac{\tan \tilde{\vartheta}'_3 + \dots}{1-\dots}}{1 - e^{-i\Xi'_{23}} \tan \tilde{\vartheta}'_2 \frac{\tan \tilde{\vartheta}'_3 + \dots}{1-\dots}}}, \quad (8a)$$

$$\beta_l^q(gg) = \frac{\tan \tilde{\vartheta}_1 + e^{-i\Xi_{12}} \frac{\tan \tilde{\vartheta}_2 + e^{-i\Xi_{23}} \frac{\tan \tilde{\vartheta}_3 + \dots}{1-\dots}}{1 - e^{-i\Xi_{23}} \tan \tilde{\vartheta}_2 \frac{\tan \tilde{\vartheta}_3 + \dots}{1-\dots}}}{1 - e^{-i\Xi_{12}} \tan \tilde{\vartheta}_1 \frac{\tan \tilde{\vartheta}_2 + e^{-i\Xi_{23}} \frac{\tan \tilde{\vartheta}_3 + \dots}{1-\dots}}{1 - e^{-i\Xi_{23}} \tan \tilde{\vartheta}_2 \frac{\tan \tilde{\vartheta}_3 + \dots}{1-\dots}}}, \quad (8b)$$

$$\beta_l'^p(ge) = \frac{1}{\{\beta_l'^p(gg)\}^*}. \quad (8c)$$

where  $\{\}^*$  means complex conjugate. Phase-factor expressions are respectively  $\Xi'_{l,l+1} = \varphi'_l - \varphi'_{l+1} + \phi'_l + \phi'_{l+1}$  and  $\Xi_{l,l+1} = \varphi_{l+1} - \varphi_l + \phi_l + \phi_{l+1}$ . Note that Eq. 8a and Eq. 8b are expressions that have the same form than the Fresnel reflection complex coefficients of a plane wave propagating through multiple planar interfaces [46].

Turning to applications, we demonstrate the capacity of composite pulses to reduce or eliminate laser-probe induced systematics on quantum interferences. We explore clock interrogation protocols limited in accuracy by laser-probe-intensity variations and atomic interferometers limited in accuracy by residual Doppler-shift and light-shift induced by pulse area modification between sets of beam splitters from different Ramsey-Bordé building-blocks. Generalized transition probabilities related to laser pulse protocols are analytically derived in

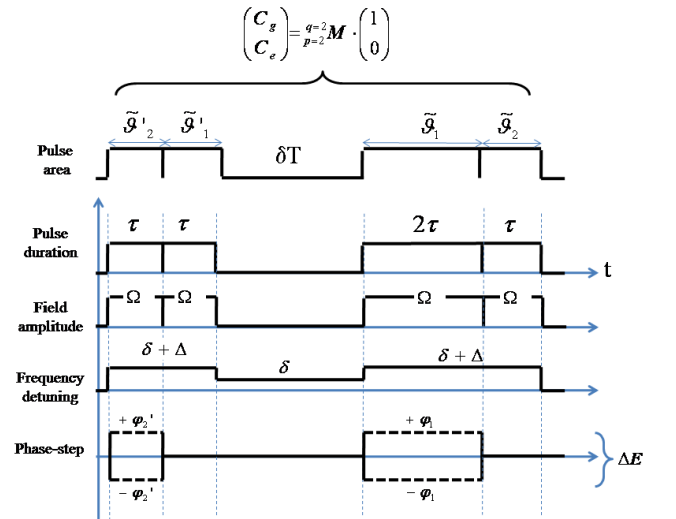


FIG. 2. (color online). Four-pulse diagrams with a single composite interaction matrix  ${}^2_2 M$  to generate R, HR- $\pi$ , GHR, HHR- $\pi$ , see Tab. I for more details. Each diagram introduces the action of pulse duration  $\tau$ , Rabi frequency  $\Omega$ , pre-compensation of the light-shift in the clock detuning  $\delta + \Delta$  and phase-step modulation  $\pm \varphi$ .

TABLE I. Composite pulse protocols for hyper-clocks. Pulse area  $\theta'_l(\theta_l)$  is given in degrees and phase-steps  $\pm\varphi'_l(\varphi_l)$  are indicated in subscript-brackets with radian unit. The standard Rabi frequency for all pulses is  $\Omega = \pi/2\tau$  where  $\tau$  is the pulse duration reference. The elementary block, used to perform calculation, is characterized by a  ${}^q_p\text{M}$  interaction matrix including  $p, q$  pulses around a single free evolution zone  $\delta T$ . Reverse protocols in time are denoted by  $(\dagger)$ .

| protocols  | composite pulse building-block ${}^q_p\text{M}$   |
|--|---|
| $\text{R}(\varphi)$<br>( $\varphi = \pi/2$ )           | $\mathbf{90}'_{\pm\varphi} \dashv \delta T \vdash \mathbf{90}_0$<br>( $\dagger$ ) $\mathbf{90}'_0 \dashv \delta T \vdash \mathbf{90}_{\mp\varphi}$  |
| $\text{HR}(\varphi)-\pi$<br>( $\varphi = \pi/2$ )      | $\mathbf{90}'_{\pm\varphi} \dashv \delta T \vdash \mathbf{180}_{\pi} \mathbf{90}_0$<br>( $\dagger$ ) $\mathbf{90}'_0 \mathbf{180}'_{\pi} \dashv \delta T \vdash \mathbf{90}_{\mp\varphi}$                                   |
| $\text{GHR}(\varphi)$<br>( $\varphi = \pi/4, 3\pi/4$ ) | $\mathbf{90}'_0 \dashv \delta T \vdash \mathbf{180}_{\pm\varphi} \mathbf{90}_0$<br>( $\dagger$ ) $\mathbf{90}'_0 \mathbf{180}'_{\mp\varphi} \dashv \delta T \vdash \mathbf{90}_0$   |
| $\text{HHR}(\varphi)-\pi$<br>( $\varphi = \pi/2$ )     | $\mathbf{90}'_{\pm\varphi} \mathbf{90}'_0 \dashv \delta T \vdash \mathbf{180}_{\pi} \mathbf{90}_0$<br>( $\dagger$ ) $\mathbf{90}'_0 \mathbf{180}'_{\pi} \dashv \delta T \vdash \mathbf{90} \vdash \mathbf{90}_{\mp\varphi}$ |

the appendix (S1 for hyper-clock interrogation scheme with one interaction matrix including  $p = q = 4$  pulses, S2 for a generalized hyper-Ramsey-Bordé (GHRB) interferometer with two interaction matrices including  $p = 1, q = 2$  pulses and S3 for a hyper-Mach-Zehnder (HMZ) configuration with a single interaction matrix including  $p = 3, q = 4$  pulses).

### III. HYPER-CLOCKS

To test our composite pulse building-block simulator, we return to the field of optical clock spectroscopy. We directly consider a four-pulse protocol for an hyper-clock with a fine tuning of the frequency shift of clock interferences. This general configuration allows us to retrieve any two-pulse or three-pulse schemes reported in Tab. I by switching-off appropriate pulse parameters from diagrams shown in Fig. 2.

For a clock configuration, we consider a single trapped ion with a very narrow optical transition confined into a Lamb-Dicke regime, i.e where Doppler and recoil shifts are eliminated [47–49]. Dispersive error signals are produced to estimate precisely the center of the interferometric resonance eliminating any shape distortion [2, 32, 34]. They are generated by applying opposite phase-steps  $\pm\varphi$  on the same transition probability  ${}^q_p\text{P}_e = 1 - {}^q_p\text{P}_g$  and computing the difference as [35, 36]:

$$\Delta E = {}^q_p\text{P}_e(\varphi) - {}^q_p\text{P}_e(-\varphi), \quad (9)$$

We establish explicitly two-level operator components from a single interaction matrix  ${}^2_2\text{M}$  to evaluate all laser

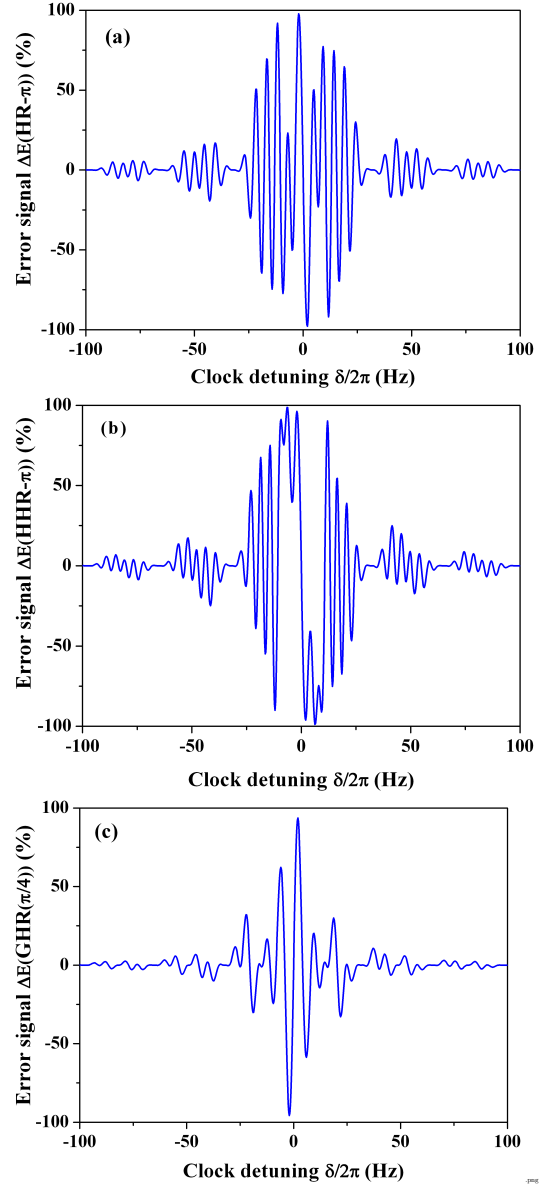


FIG. 3. (color online). Typical  $\Delta E$  dispersive error signals generated with our computational algorithm based on a simulation of the  ${}^{171}\text{Yb}^+$  ion clock interrogation with protocols from Tab. I. (a)  $\text{HR}-\pi$  with 3 pulses. (b)  $\text{HHR}-\pi$  with 4 pulses. (c)  $\text{GHR}(\pi/4)$  with 3 pulses. Laser pulse parameters are  $\tau = 30.5\text{ms}$ , free evolution times around  $T = 122\text{ms}$  under a mean compensated light-shift of  $\Delta_{LS}/2\pi = 95\text{Hz}$ . A mean Rabi frequency  $\Omega/2\pi = 8.20\text{Hz}$  is fixed as in [51].

pulse hyper-clock protocols reported in Tab. I. The matrix coefficients  ${}^2_2C_{gg}, {}^2_2C_{ge}$  driving a four-pulse probe interrogation scheme are computed using the following el-

ements:

$$\alpha_1'^2(gg) = \left( \prod_1^{p=2} \cos \tilde{\vartheta}_l e^{i\phi_l'} \right) \cdot (1 - S'_{2,2}), \quad (10a)$$

$$\alpha_1^2(gg) = \left( \prod_1^{q=2} \cos \tilde{\vartheta}_l e^{i\phi_l} \right) \cdot (1 - S_{2,2}), \quad (10b)$$

$$\alpha_1'^2(ge) = -ie^{-i(\phi_2' + \varphi_2' + \Xi_2')} \cdot \left( \prod_1^{p=2} \cos \tilde{\vartheta}_l e^{i\phi_l'} \right) \cdot (S'_{2,1}), \quad (10c)$$

We have respectively for  $S'_{2,2}(gg)$ ,  $S'_{2,1}(ge)$  and  $S_{2,2}(gg)$ :

$$S'_{2,2} = e^{-i\Xi'_{12}} \tan \tilde{\vartheta}_1 \tan \tilde{\vartheta}_2, \quad (11a)$$

$$S'_{2,1} = \tan \tilde{\vartheta}_1 + e^{i\Xi'_2} \tan \tilde{\vartheta}_2, \quad (11b)$$

$$S_{2,2} = e^{-i\Xi_{12}} \tan \tilde{\vartheta}_1 \tan \tilde{\vartheta}_2, \quad (11c)$$

The corresponding complex phase factor  $\beta_1'^2(gg)$ ,  $\beta_1^2(gg)$  leading to a phase-shift correction are:

$$\beta_1'^2(gg) = \frac{\tan \tilde{\vartheta}_1 + e^{-i\Xi'_{12}} \tan \tilde{\vartheta}_2}{1 - e^{-i\Xi'_{12}} \tan \tilde{\vartheta}_1 \tan \tilde{\vartheta}_2}, \quad (12a)$$

$$\beta_1^2(gg) = \frac{\tan \tilde{\vartheta}_1 + e^{-i\Xi_{12}} \tan \tilde{\vartheta}_2}{1 - e^{-i\Xi_{12}} \tan \tilde{\vartheta}_1 \tan \tilde{\vartheta}_2}, \quad (12b)$$

$$\beta_1'^2(ge) = \frac{1}{\{\beta_1'^2(gg)\}^*}, \quad (12c)$$

We give the decomposition of phase factor expressions as following:

$$\Xi'_1 = 0 \quad (13a)$$

$$\Xi'_2 \equiv \Xi'_{12} \quad (13b)$$

$$\Xi'_{12} = \varphi'_1 - \varphi'_2 + \phi'_1 + \phi'_2, \quad (14a)$$

$$\Xi_{12} = \varphi_2 - \varphi_1 + \phi_1 + \phi_2. \quad (14b)$$

See also [50] as another computational way to obtain directly  ${}^2C_{ge}$  from  ${}^2C_{gg}$ .

The transition probability can be detected by measuring the atomic population fraction in the ground state or flipping to the excited state. Hyper-Ramsey (HR- $\pi$ ) and generalized hyper-Ramsey GHR( $\pi/4$ ) protocols with 3 pulses are compared to a new hybrid hyper-Ramsey (HHR- $\pi$ ) protocol using four pulses from Tab. I. We employ the Beloy's model to analyze laser-probe-intensity fluctuation between repetitive sequences of composite pulses for clock interrogation [51]. Typical dispersive shapes for  $\Delta E$  are presented in Fig. 3 (a), (b) and (c). The fractional clock error, related to the specific electric octupole (E3) clock transition of a single trapped ion  ${}^{171}\text{Yb}^+$ , is reported in Fig. 4 (a) and (b). The robustness of the HR protocol is exhibiting a relative quartic

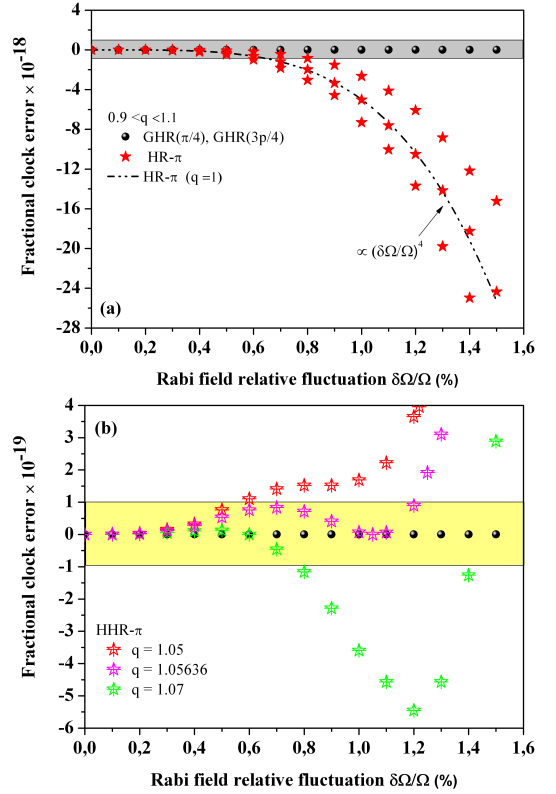


FIG. 4. (color online). Fractional clock error versus relative probe-laser fluctuation  $\delta\Omega/\Omega$ . (a) HR- $\pi$  protocol ( $\star$  full red colored stars and dashed line). (b) HHR- $\pi$  protocol (open multi-colored  $\star$  stars) with an additional  $90^\circ$  laser pulse after the first one. We also report GHR( $\pi/4$ ), GHR( $3\pi/4$ ) protocols ( $\bullet$  black dots) for comparison to (a) and (b) plots. Laser pulse parameters as in Fig. 3 where pulse area variation  $\Omega\tau = q\pi/2$  is driven by the parameter  $q$  from 0.9 to 1.1 as described in [51]. Note the change in scale between the region in grey indicating a fractional clock-frequency shift correction at the  $10^{-18}$  and the yellow region for a  $10^{-19}$  level of relative accuracy.

sensitivity to the Rabi field fluctuation  $\delta\Omega/\Omega$ (%) initially predicted by [51] while a GHR( $\pi/4$ ) (or equivalently GHR( $3\pi/4$ )) protocol does not suffer from any residual light-shift correction even for a constrained  $\pm 10\%$  pulse area variation. As expected, the HR fractional clock correction requires a laser field control below 0.5% (intensity below 1%) to reach a  $-5 \times 10^{-19}$  relative accuracy (grey region). In Fig. 4(a) and (b), a new HHR- $\pi$  protocol which uses an additional  $90^\circ$  laser pulse immediately after the first  $90^\circ_{\pm\pi/2}$  phase-shifted Ramsey pulse is modifying the expected clock fractional error through a fine tuning control of the pulse area.

This additional pulse is not only able to remove the quartic dependance of the HR- $\pi$  fractional clock error with the laser field fluctuation but is also capable of changing the sign of the clock frequency-shift. Inspired by the precise tuning control of residual high-order light-shifts in optical lattices offered by the trap depth [52],



we have investigated the pulse area control within the variation of the Rabi frequency through the  $q$  parameter changed from 0.9 to 1.1 in Fig. 4(a) and from 1.05 to 1.07 in Fig. 4(b). Several "magic" values of the mean Rabi frequency  $\Omega\tau = q_m\pi/2$ , if well controlled, can be used with HHR- $\pi$  protocol to remove clock sensitivity to laser amplitude fluctuation. For example, from Fig. 4(b), we get  $q_m = 1.05636$  where a cancelation of the fractional clock error at the  $10^{-20}$  level (yellow region) seems possible for a frequency fluctuation at the 1% level. If our Rabi frequency fluctuation is pushed below 0.6%, the value  $q_m = 1.07$  seems a better choice. In any case, the GHR protocol remains very robust as long as the phase-step is precisely controlled as seen in Fig. 4(a) and (b) since the residual part of the compensated light-shift is removed at all order in the clock detuning [53]. Note that another hybrid error signal  $\Delta E_{\text{HGH}}$  can be generated by mixing GHR( $\pi/4$ ) and GHR( $3\pi/4$ ) schemes in the following way [36]:

$$\Delta E_{\text{HGH}} = \frac{1}{2} (\Delta E_{\text{GHR}(\pi/4)} - \Delta E_{\text{GHR}(3\pi/4)}). \quad (15)$$

Combining error signals are still offering better robustness for example to the signal distortion from ion motion heating in a single ion rf trap. A potential fractional clock error around  $5 \times 10^{-20}$  was estimated following Eq. 15 in comparison to the original HR- $\pi$  protocol [54]. It has been also recently demonstrated that GHR( $\pi/4$ ) and GHR( $3\pi/4$ ) schemes have a strong robustness against residual light-shift coupled to spontaneous emission in an optically dense medium of cold atoms [55]. Indeed, there is a large possibility of unexplored exotic composite pulse protocols for optical clocks due to the richness of the quantum Hilbert space engineering [56, 57].

#### IV. HYPER-INTERFEROMETERS

We propose now to transfer composite pulse protocols, developed in the time-domain for hyper-clocks, to spatial-domain interferometry. We focus on the field of atomic matter-wave interferometers where the two-pulse Ramsey configuration is still an elementary building block of more elaborated successive interrogation schemes including external degrees of freedom with Doppler and recoil shifts and a residual uncompensated light-shift in the detuning.

The mechanical effects of light pulses were initially based on single photon transitions and exploited as beam-splitters or mirrors to spatially separate or recombine atomic or molecular wavepackets [6, 8, 41]. Stimulated Raman transitions in a microwave excitation by two-photon processes were pioneered by Kasevich and Chu for internal state manipulation of alkali species [12–15, 18] while Bragg diffraction was preferred to eliminate potential action of one photon light-shift in atomic states but requiring narrow momentum distribution to be very efficient [58–60]. Stimulated Raman optical transitions in

bosonic alkaline-earth quantum systems such as Yb, Hg, Sr and Mg have been already proposed as ultra-robust two-photon hyper clocks against detrimental light-shift and Zeeman effect [61]. All optical composite-pulse two-photon interferometry might thus be considered by inserting laser phase-steps, Doppler shift and atomic recoil state labeling in analogy with velocity-selective stimulated Raman transitions in alkali atoms [62].

However, in all types of coherent Raman or Bragg manipulation of matter-waves, degraded performances of interferometers often rely on imperfect overlapping of wavepackets due to phase-shift accumulation during light pulses [63–66]. Revisiting Ramsey-Bordé matter-wave interferometry is motivated by the application of composite phase-shifts from Eq. 7a and Eq. 7b to compensate simultaneously for residual light-shifts associated to non vanishing Doppler-shifts when laser pulse area is drifting between pairs of atomic beam splitters.

Several types of interferometers have been developed from devices sensitive to recoil frequency or devices measuring inertial effects like rotation or acceleration. Composite pulses with Bragg or stimulated Raman type transitions and butterfly geometry with four pulses have already been employed to improve current cold-atom gyroscopes in sensitivity and accuracy to rotations [67, 68]. Here, sophisticated sequences of pulses with phase-steps are rather proposed to shield matter-wave interferences against pulse defects inside atomic interferometers.

In this context, we study an asymmetric Ramsey-Bordé (RB) configuration used to determine the fine structure constant for fundamental test in QED [17, 41] and a Mach-Zehnder (MZ) interferometer for iner-

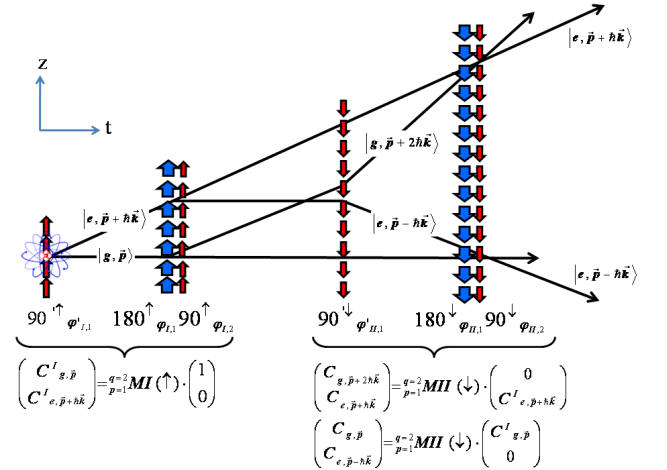


FIG. 5. (color online). Generalized hyper-Ramsey-Bordé (GHRB) interferometer with multiple traveling waves designed by  $p$  and  $q$  composite pulses. Two counter-propagating sets of three co-propagating composite laser pulses are introduced by interaction zones  ${}^2\text{MI}(\uparrow)$  and  ${}^2\text{MI}(\downarrow)$  where  $\uparrow\downarrow$  arrows are corresponding to  $kv_z$  transverse Doppler orientation. Laser pulse phases for each set are indicated respectively by  $\varphi_i^I(\varphi_i^I)$  with  $\uparrow$  and  $\varphi_i^{II}(\varphi_i^{II})$  with  $\downarrow$ .

TABLE II. Composite pulses interrogation protocols for hyper-Ramsey-Bordé atom interferometry. Pulse area  $\theta'_l(\theta_l)$  is given in degrees and phase-steps  $\pm\varphi'_l(\varphi_l)$  are indicated in subscript-brackets with radian unit. The standard Rabi frequency for all pulses is  $\Omega = \pi/2\tau$  where  $\tau$  is the pulse duration reference. Free evolution time regions are given by  $\delta^\uparrow T$  ( $\delta^\downarrow T$ ) where  $\uparrow\downarrow$  denotes the transverse Doppler-shift orientation. Each elementary building-block  ${}^q\text{MI}(\uparrow)(\downarrow)$  and  ${}^q\text{MII}(\downarrow)(\uparrow)$  are separated by the intermediate  $\delta^\uparrow T'$  or  $\delta^\downarrow T'$  free evolution zone. Reverse protocols in time are denoted by  $(\dagger)$ .

| protocols   | composite pulse building-blocks ${}^q\text{MI}(\uparrow)(\downarrow)$ , ${}^q\text{MII}(\downarrow)(\uparrow)$   |
|---|--|
| RB( $\varphi$ )<br>( $\varphi = \pi/4$ )                  | $\mathbf{90}'_{\pm\varphi} \dashv \delta^\uparrow T \vdash \mathbf{90}_0^\uparrow \dashv \delta^\uparrow T' \vdash \mathbf{90}'_{\pm\varphi} \dashv \delta^\downarrow T \vdash \mathbf{90}_0^\downarrow$<br>( $\dagger$ ) $\mathbf{90}_0'^\downarrow \dashv \delta^\downarrow T \vdash \mathbf{90}_{\mp\varphi}^\downarrow \dashv \delta^\downarrow T' \vdash \mathbf{90}_0'^\uparrow \dashv \delta^\uparrow T \vdash \mathbf{90}_{\mp\varphi}^\uparrow$   |
| HRB( $\varphi$ ) $-\pi$<br>( $\varphi = \pi/4$ )          | $\mathbf{90}'_{\pm\varphi} \dashv \delta^\uparrow T \vdash \mathbf{180}_\pi^\uparrow \mathbf{90}_0^\uparrow \dashv \delta^\uparrow T' \vdash \mathbf{90}'_{\pm\varphi} \dashv \delta^\downarrow T \vdash \mathbf{180}_{\mp\varphi}^\downarrow \mathbf{90}_0^\downarrow$<br>( $\dagger$ ) $\mathbf{90}_0'^\downarrow \mathbf{180}_\pi'^\downarrow \dashv \delta^\downarrow T \vdash \mathbf{90}_{\mp\varphi}^\downarrow \dashv \delta^\downarrow T' \vdash \mathbf{90}_0'^\uparrow \mathbf{180}_\pi'^\uparrow \dashv \delta^\uparrow T \vdash \mathbf{90}_{\mp\varphi}^\uparrow$                  |
| GHRB( $\varphi$ )<br>( $\varphi = \pi/8, 3\pi/8$ )        | $\mathbf{90}_0'^\uparrow \dashv \delta^\uparrow T \vdash \mathbf{180}_{\pm\varphi}^\uparrow \mathbf{90}_0^\uparrow \dashv \delta^\uparrow T' \vdash \mathbf{90}_0'^\downarrow \dashv \delta^\downarrow T \vdash \mathbf{180}_{\pm\varphi}^\downarrow \mathbf{90}_0^\downarrow$<br>( $\dagger$ ) $\mathbf{90}_0'^\downarrow \mathbf{180}_{\mp\varphi}^\downarrow \dashv \delta^\downarrow T \vdash \mathbf{90}_0^\downarrow \dashv \delta^\downarrow T' \vdash \mathbf{90}_0'^\uparrow \mathbf{180}_{\mp\varphi}^\uparrow \dashv \delta^\uparrow T \vdash \mathbf{90}_0^\uparrow$                 |
| GHRB( $\varphi$ ) $-\pi$<br>( $\varphi = \pi/8, 3\pi/8$ ) | $\mathbf{90}_\pi'^\uparrow \dashv \delta^\uparrow T \vdash \mathbf{180}_{\pm\varphi}^\uparrow \mathbf{90}_\pi^\uparrow \dashv \delta^\uparrow T' \vdash \mathbf{90}_\pi'^\downarrow \dashv \delta^\downarrow T \vdash \mathbf{180}_{\pm\varphi}^\downarrow \mathbf{90}_\pi^\downarrow$<br>( $\dagger$ ) $\mathbf{90}_\pi'^\downarrow \mathbf{180}_{\mp\varphi}^\downarrow \dashv \delta^\downarrow T \vdash \mathbf{90}_\pi^\downarrow \dashv \delta^\downarrow T' \vdash \mathbf{90}_\pi'^\uparrow \mathbf{180}_{\mp\varphi}^\uparrow \dashv \delta^\uparrow T \vdash \mathbf{90}_\pi^\uparrow$ |

tial measurement [21, 64]. We apply composite pulse protocols to realize a generalized hyper-Ramsey-Bordé (GHRB) interferometer reducing or eliminating residual corrections from light-shift and sensitivity to residual transverse Doppler-shifts. We also present an hyper-Mach-Zehnder (HMZ) interferometer to strongly reduce the sensitivity against detrimental modification in pulse area variation between beam splitters investigated in [64] and more recently reported for a symmetric Ramsey-Bordé configuration [65].

### A. HYPER RAMSEY-BORDÉ

The original Ramsey-Bordé (RB) interferometer is based on a four-laser pulse configuration, as reported in first line of Tab. II. If the motion of atoms is taking into account, the first Ramsey two-zone setup denoted as  ${}^1\text{MI}(\uparrow)$ , recovers a strong sensitivity to the transverse first-order Doppler effect. While, with microwaves or radio-frequencies, the atomic wavepackets are still interfering after a single Ramsey two-pulse interrogation, fringes are destroyed by optical frequencies with large wavevectors. Indeed, the splitting between wavepackets is velocity dependent and becomes too large requiring a Doppler cancelation technique to close the interferometer to avoid the lost of quantum interferences. Bordé proposed in the 1980's a configuration with four traveling waves consisting of two separated Ramsey two-zones  ${}^1\text{MI}(\uparrow)$  and  ${}^1\text{MII}(\downarrow)$  where arrows are describing two counter-propagating sets of co-propagating laser pulses [6]. Within this interaction geometry, opposite sets of laser pulse wavevectors cancel the Doppler-shift and Ramsey interferences are retrieved at the output of the interferometer [41].

Inserting composite pulses in atomic interferometry is motivated by eliminating potential uncompensated residual part of Doppler-shift sensitivity and light-shift on a recoil frequency determination when the pulse area changes over the whole pulse interrogation. Indeed, for an original RB interferometer, a uniform distribution of laser amplitude over the full sequence will be rejected by a differential measurement between the two sets of shifted wavepackets. These terms drop out in any interferometric comparison between paths. However, if pulse area of pairs of beam splitters are modified between two Ramsey-Bordé interaction zones, a small parasitic shift may be recovered.

We consider our two-level system interacting with an arbitrary number of traveling waves which may propagate in opposite direction. Following the decomposition rules with multiple interrogation zones from the previous section, the interaction geometry of a robust hyper-interferometer (HRB $-\pi$  and GHRB) is divided into two composite pulse building-blocks with interaction matrices  ${}^2\text{MI}(\uparrow)$  and  ${}^2\text{MII}(\downarrow)$  separated by an intermediate free evolution time  $T'$  as shown in Fig. 5 and listed in Tab. II. The components of each interaction matrix required to compute each amplitude of probability associated to different path trajectories of wavepackets are given in section S2 from the appendix.

We evaluate first complex coefficients  ${}^q C_{g, \vec{p}}^I(t)$  and  ${}^q C_{e, \vec{p} + \hbar \vec{k}}^I(t)$  within the first Ramsey zone  ${}^1\text{MI}(\uparrow)$  with  $p = 1$  and  $q = 2$  pulses. Then we evaluate complex coefficients for the second interaction zone  ${}^2\text{MI}(\downarrow)$  starting from previous solutions of interfering trajectories closing the interferometer. The first hyper-Ramsey-Bordé  ${}^2\text{MI}(\uparrow)$  building-block is thus computed taking

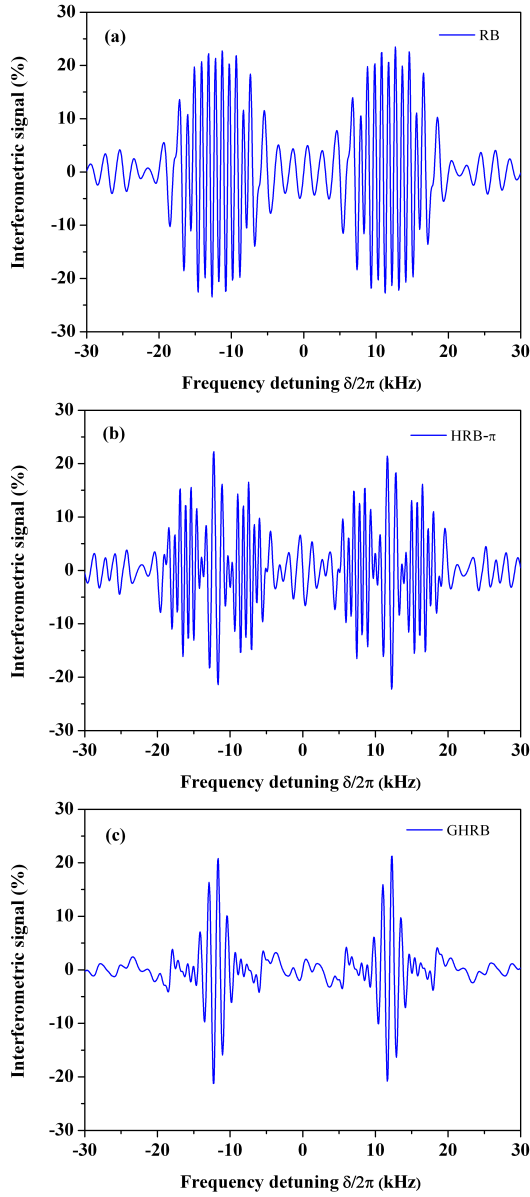


FIG. 6. (color online). Resolving the  $^{40}\text{Ca}$  recoil doublet with matter-wave composite pulse interferometry integrated over a narrow gaussian transverse velocity distribution around  $T = 250$  pK versus frequency detuning  $\delta/2\pi$ . (a) RB fringes. (b) HRB- $\pi$  fringes. (c) GHRB fringes. Laser pulse duration is  $\tau = 0.1\text{ms}$  and free evolution times around  $T = 30/\delta_r$  where we apply for the intermediate free evolution time  $T' \rightarrow 0$  and  $\delta_r = \hbar k^2/2m$ .

$C_{g,\vec{p}}(0) = 1, C_{e,\vec{p}+\hbar\vec{k}}(0) = 0$  and gives:

$${}^2_1C_{g,\vec{p}}^I(t) = {}^2_1C_{gg}^I, \quad (16a)$$

$${}^2_1C_{e,\vec{p}+\hbar\vec{k}}^I(t) = {}^2_1C_{eg}^I = -{}^2_1C_{ge}^{I*}, \quad (16b)$$

where  $*$  means complex conjugate. The common laser detuning  $\delta_I$  for all spinor matrix component in  ${}^2_1\text{MI}(\uparrow)$  zone is defined in section S2 from the appendix. At the end of this first GHRB  ${}^2_1\text{MI}(\uparrow)$  interaction zone, wavepack-

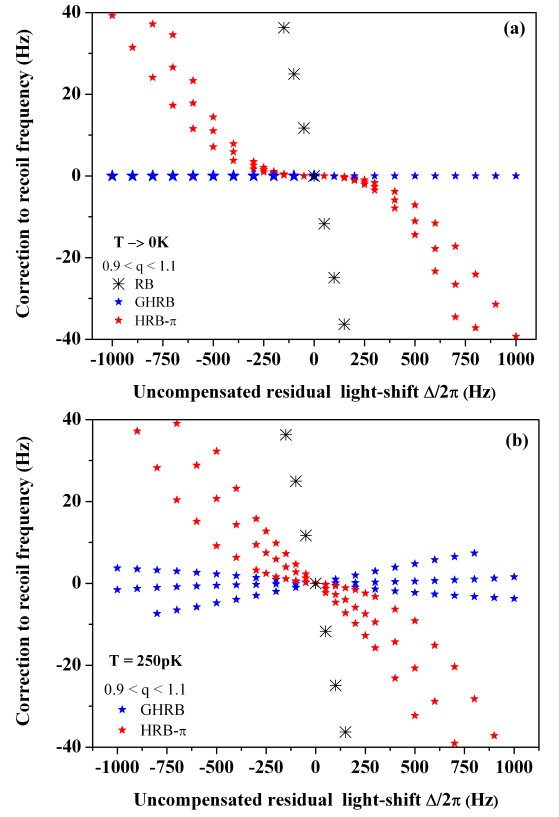


FIG. 7. (color online). (a) Numerical tracking of the error signal frequency position for HRB- $\pi$  and GHRB protocols around zero for various uncompensated part of the residual light-shift for  $T \rightarrow 0\text{K}$ . (b) Distortion effect of matter-waves due to a non zero temperature after integration over a narrow gaussian transverse velocity distribution around  $T = 250$  pK. All tracking points are generated with same parameters as in Fig. 6 except pulse area variation  $\Omega\tau = q\pi/2$  which is driven by the parameter  $q$  from 0.9 to 1.1. between the two interaction zones  ${}^2_1\text{MI}(\uparrow), {}^2_1\text{MI}(\downarrow)$ .

ets are separated in several components in space during an intermediate  $T'$  free evolution time. This is seen as a simple additional phase-factor of the form  $e^{\pm i\delta T'/2}$ . In asymmetric or symmetric Ramsey-Bordé interferometers, this delay allows for Bloch-oscillations to transfer large number of photon momenta to the wavepackets [17, 18].

The final complex GHRB matter-wave amplitudes  ${}^2_1C_{e,\vec{p}-\hbar\vec{k}}(t)$  and  ${}^2_1C_{e,\vec{p}+\hbar\vec{k}}(t)$  after successive interaction with  ${}^2_1\text{MI}(\uparrow)$  and  ${}^2_1\text{MI}(\downarrow)$  regions are four overlapping wavepackets centered at the recoil frequency  $\pm\delta_r$  ( $\pm\hbar\vec{k}$ ) [41]. The final GHRB amplitude of the wavefunction after successive interaction is now given by:

$${}^2_1C_{e,\vec{p}-\hbar\vec{k}}(t) = -{}^2_1C_{ge}^{II*} \cdot {}^2_1C_{gg}^I, \quad (17a)$$

$${}^2_1C_{e,\vec{p}+\hbar\vec{k}}(t) = -{}^2_1C_{gg}^{II*} \cdot {}^2_1C_{ge}^{I*}, \quad (17b)$$

After algebraic manipulation, one up-shifted wavepacket



expression  ${}^2_1C_{e,\vec{p}-\hbar\vec{k}}(t)$  is expressed as:

$${}^2_1C_{gg}^I = {}^2_1\alpha_{gg}^I e^{i\delta_I T/2} \left[ 1 - |\beta_{gg}^I|^2 e^{-i(\delta_I T + {}^2_1\Phi_{gg}^I)} \right], \quad (18a)$$

$${}^2_1C_{ge}^{II*} = {}^2_1\alpha_{ge}^{II*} e^{-i\delta_{II} T/2} \left[ 1 + |\beta_{ge}^{II*}|^2 e^{i(\delta_{II} T + {}^2_1\Phi_{ge}^{II*})} \right], \quad (18b)$$

where  $\alpha_{ge}^{II*}, \beta_{ge}^{II*}$  components from  ${}^2_1C_{ge}^{II*}$  are analytically derived with the proper detuning definition  $\delta_{II}$  from appendix section S2. The other down-shifted wavepacket expression  ${}^2_1C_{e,\vec{p}+\hbar\vec{k}}(t)$  is:

$${}^2_1C_{gg}^{I*} = {}^2_1\alpha_{gg}^{I*} e^{-i\delta_I T/2} \left[ 1 + |\beta_{gg}^{I*}|^2 e^{i(\delta_I T + {}^2_1\Phi_{gg}^{I*})} \right], \quad (19a)$$

$${}^2_1C_{gg}^{II*} = {}^2_1\alpha_{gg}^{II*} e^{-i\delta_{II} T/2} \left[ 1 - |\beta_{gg}^{II*}|^2 e^{i(\delta_{II} T + {}^2_1\Phi_{gg}^{II*})} \right]. \quad (19b)$$

while  $\alpha_{gg}^{II*}, \beta_{gg}^{II*}$  components from  ${}^2_1C_{gg}^{II*}$  are derived with the proper detuning definition  $\delta_{II}$  also reported in appendix section S2.

Matter-wave interferences are centered around a high-frequency (HF) recoil term  ${}^2_1C_{g,\vec{p}-\hbar\vec{k}}(t)$  and a low-frequency (LF) recoil term  ${}^2_1C_{e,\vec{p}+\hbar\vec{k}}(t)$  where we have identified composite phase-shifts as:

$${}^2_1\Phi_{e,\vec{p}-\hbar\vec{k}} = \varphi_L + \phi_L - (\text{Arg}[{}^2_1\beta_{gg}^I] + \text{Arg}[{}^2_1\beta_{ge}^{II}]), \quad (20a)$$

$${}^2_1\Phi_{e,\vec{p}+\hbar\vec{k}} = \varphi_L + \phi_L - (\text{Arg}[{}^2_1\beta_{ge}^I] + \text{Arg}[{}^2_1\beta_{gg}^{II}]), \quad (20b)$$

with a phase composition  $\varphi_L + \phi_L$  given by [37]:

$$\varphi_L = \varphi_L^I + \varphi_L^{II} = \varphi_1^I - \varphi_1'^I + \varphi_1^{II} - \varphi_1'^{II}, \quad (21a)$$

$$\phi_L = \phi_L^I + \phi_L^{II} = \phi_1'^I + \phi_1^I + \phi_1'^{II} + \phi_1^{II}, \quad (21b)$$

These composite phase-shift expressions are also consistent with a graphical representation of strong-field density matrix diagrams related to low and high frequency recoil peaks of Ramsey-Bordé fringes when additionnal interaction matrices are taken in to account [41–43]. Our computational algorithm allows us to derive an analytical formulae of the composite phase-shift directly acting on matter-wave interferences based on asymmetrical generalized hyper-Ramsey-Bordé interferometer. The overall effect of the residual uncompensated part of the light-shift remnant to the original Ramsey-Bordé scheme is finally encoded in Eq. 21b. Results based on Eq. 20a and Eq. 20b are generalizing the usual description of atom interferometers neglecting potential light-shift distortion.

Note that there is also the RB interferometer configuration where the last set of optical traveling waves used to close the interferometer are not reversed. This symmetric Ramsey-Bordé interferometer is also exploited for the fine structure determination [18, 66]. Such a geometry is not sensitive to the net frequency dependence of the interference signal such that the relative phase-shift

accumulation between arms of this symmetrical RB configuration is given by [37]:

$$\varphi_L = \varphi_L^I - \varphi_L^{II} = \varphi_1^I - \varphi_1'^I + \varphi_1'^{II} - \varphi_1^{II}, \quad (22a)$$

$$\phi_L = \phi_L^I - \phi_L^{II} = \phi_1'^I + \phi_1^I - \phi_1'^{II} - \phi_1^{II}. \quad (22b)$$

It is interesting to note that the sensitivity to residual Doppler-shifts and light-shifts are equivalently coming from Eq. 21b for an asymmetric interferometer and from Eq. 22b for a symmetric configuration. These terms are responsible for a velocity-dependent phase-shift leading to an imperfect overlapping of wavepackets originally derived in [65].

Coming back to the asymmetric RB interferometer, the generalized hyper-Ramsey Bordé transition probability is thus given by:

$${}^2_1P_{e,\vec{p}\pm\hbar\vec{k}} = \left| {}^2_1C_{e,\vec{p}\pm\hbar\vec{k}}(t) \right|^2, \quad (23)$$

Similar to the generation of error signals based on Eq. 9, we also generate dispersive fringes as following:

$$\Delta E = {}^2_1P_{e,\vec{p}\pm\hbar\vec{k}}(\varphi) - {}^2_1P_{e,\vec{p}\pm\hbar\vec{k}}(-\varphi). \quad (24)$$

where we can apply phase-step protocols reported in Tab. II. Combination of phase-step protocols within two successive building-blocks following Eq. 21a, required to produce dispersive error signals, are using half values needed for an hyper-clock interrogation scheme based on a single building-block.

The extraction of the composite phase-shift from analytical expressions of error signal shapes is not always an easy task and sometimes requires a numerical tracking of the central dispersive feature. In the following figures that we have produced, we have numerically plotted the error signal and associated frequency-shifts for an accurate evaluation of interference distortion. We have also checked that nonlinear effects leading to these distortions are effectively related in many part to the corrections resulting from Eq. 20a and Eq. 20b.

Dispersive errors signals based on hyper-Ramsey-Bordé (HRB- $\pi$ ) and generalized hyper-Ramsey-Bordé (GHRB) protocols from Tab. II are generated following Eq. 24. The last error signal  $\Delta E_{\text{GHRB}}$  reported in Fig. 6(c) is built by a combination of  $\pm\pi/8$  and  $\pm3\pi/8$  phase-steps:

$$\Delta E_{\text{GHRB}} = \frac{1}{2} (\Delta E_{\text{GHRB}(\pi/8)} - \Delta E_{\text{GHRB}(3\pi/8)}), \quad (25)$$

Associating two error signals in a cooperative manner is a robust way to reduce again residual uncompensated Doppler-shifts and light-shifts coupled to pulse area variation between multiple building-blocks with better efficiency than a single error signal [35].

We report typical dispersive error signals integrated over a narrow transverse gaussian velocity distribution around  $T = 250$  pK using Ca atomic parameters as example in Fig. 6(a) for the RB interrogation scheme, (b) for

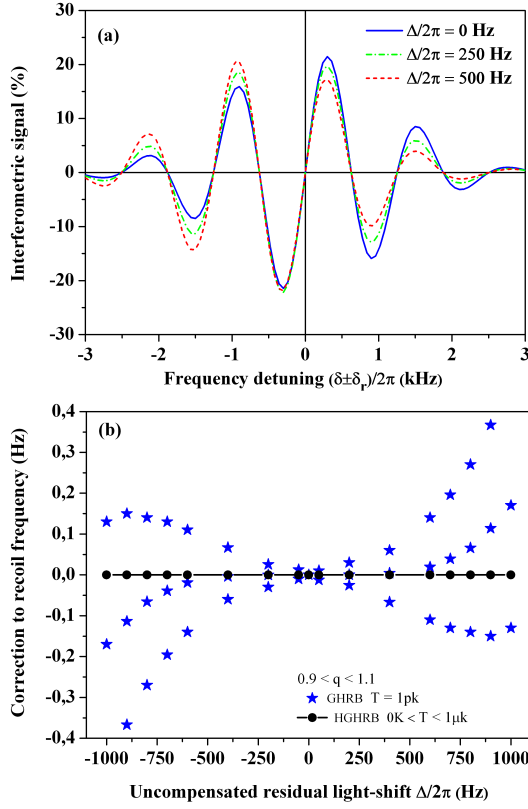


FIG. 8. (color online). (a) Typical HGHRB error signal versus frequency detuning  $\delta/2\pi$  (Hz) centered around each recoil frequency and integrated over various narrow gaussian velocity distributions between  $0 < T < 1 \mu\text{K}$  for different uncompensated part of residual light-shift  $\Delta/2\pi$ . (b) Frequency correction to the recoil with the HGHRB protocol versus uncompensated part of the residual light-shift  $\Delta/2\pi$  over a wide distribution of ultra-cold temperatures between  $0 < T < 1 \mu\text{K}$  (Black solid line and dots  $\bullet$ ). Blue stars  $\star$  represents the frequency correction to the recoil from a single GHRB protocol integrated over a narrow gaussian velocity distribution around  $T = 1 \text{ pK}$ . All Numerical tracking points are generated with same parameters as in Fig. 6 except pulse area variation  $\Omega\tau = q\pi/2$  which is driven by the parameter  $q$  from 0.9 to 1.1 between the two interaction zones  $^1\text{MI}(\uparrow)$ ,  $^2\text{MII}(\downarrow)$ .

the HRB- $\pi$  protocol and in (c) for the GHRB protocol. Matter-waves are all split in two wavepackets that are separated by the atomic doublet recoil doublet  $\sim 23 \text{ kHz}$  for Ca.

We have also plotted the correction to the recoil due to residual light-shifts for two different transverse velocity distributions of the wave packet. In the ideal case  $T \rightarrow 0 \text{ K}$  presented in Fig. 7(a), the HRB- $\pi$  interferometric scheme exhibits a highly nonlinear cubic dependence of the recoil correction under residual uncompensated parts of the light-shift  $\Delta/2\pi$ . As expected, the GHRB scheme is still completely removing the dependence in the residual light-shift at all order in the detuning. However, the assumption that a sample of trapped

atoms are in the  $T \rightarrow 0 \text{ K}$  regime is unrealistic.

By integrating the interferometric error signal over a transverse gaussian distribution of velocities at  $T = 250 \text{ K}$  as shown in Fig. 7(b), the nonlinear compensation of the residual light-shift is lost and a small linear dependence of the recoil correction with  $\Delta/2\pi$  is restored for both protocols. A small asymmetry in pulse area between the two sets of Ramsey-Bordé interaction zones also generate a small sensitivity to potential light-shifts. However, let us remark that it is possible to cool atomic samples to ultra-cold temperatures relying on delta-kick techniques or sub-recoil cooling to reach nK to pK temperatures with very narrow momentum dispersion [73, 74]. Reaching lower temperature is thus an additional benefit for robust matter-wave interferometry with composite pulses.

In order to make an error signal more robust, even at relatively higher temperatures, to residual light-shifts and pulse area errors between interaction zones coupled to the transverse atomic motion, we present a new hybrid GHRB error signal (HGHRB) based on the following protocol:

$$\Delta E_{\text{HGHRB}} = \frac{1}{2} (\Delta E_{\text{GHRB}} + \Delta E_{\text{GHRB}-\pi}). \quad (26)$$

Such a combination of phase-shifted signals by  $\pi$ , reported in Tab. II, is cooperatively adding interference fringes [69] with opposite phase-shifts to completely cancel any residual light-shifts and transverse Doppler-shifts. We check that symmetric or asymmetric residual light-shifts equivalent to residual Doppler-shifts with opposite wavevectors between  $^1\text{MI}(\uparrow)$  and  $^2\text{MII}(\downarrow)$  building-blocks are canceled when pulse area is changing by  $\pm 10\%$ .

We now plot our new dispersive error signal in Fig. 8(a) versus the clock detuning  $\delta/2\pi$  centered around each recoil frequency component for different residual light-shifts and large transverse temperatures  $0 < T < 1 \mu\text{K}$ . The robustness of the recoil correction to the residual light-shift coupled to pulse area variation by  $\pm 10\%$  is presented in Fig. 8(b). The solid blue stars are the numerical tracking of the error signal near the recoil frequency for a GHRB scheme working at a transverse temperature around  $= 1 \text{ pK}$ . The solid black line with dots is the error signal correction from the hybrid scheme HGHRB based on Eq. 26. The combination of GHRB and GHRB- $\pi$  sequences are acting like a Hahn spin-echo compensation against pulse area variation coupled to residual light-shifts and transverse Doppler-shifts. Finally, note that a class of mirror-like interrogation schemes is reported Tab. II denoted as  $(\dagger)$  protocols. It is realized by applying a change in pulse order requiring also a sign flip in laser phase-step as  $\varphi \mapsto -\varphi$ . Association of GHRB and GHRB $(\dagger)$  schemes are motivated by a potential elimination of dissipation-induced residual frequency-shifts investigated for hyper-clocks [35].

TABLE III. Composite pulses interrogation protocols for an hyper Mach-Zehnder interferometer. The elementary block, used to perform calculation, is still characterized by a single  ${}_p^q\mathbf{M}$  interaction matrix. Arrow  $\uparrow$  denotes the detuning corrected by Doppler-shift and recoil absorption within composite pulses and during free evolution time. Reverse protocols in time are also denoted by  $(\dagger)$  where  $\text{HMZ}(\varphi)$  and  $\text{HMZ}(-\varphi)$  are their own time-reflection.

| protocols              | composite pulse building-block ${}_p^q\mathbf{M}(\uparrow)$  |
|------------------------|--|
| $\text{MZ}(\varphi)$   | $\mathbf{90}_\varphi'^\uparrow \dashv \delta^\uparrow \mathbf{T} \vdash \mathbf{180}_0^\uparrow \dashv \delta^\uparrow \mathbf{T} \vdash \mathbf{90}_0^\uparrow$   |
|                        | $(\dagger) \mathbf{90}_0'^\uparrow \dashv \delta^\uparrow \mathbf{T} \vdash \mathbf{180}_0^\uparrow \dashv \delta^\uparrow \mathbf{T} \vdash \mathbf{90}_{-\varphi}^\uparrow$  |
|                        | $\mathbf{90}_\varphi'^\uparrow \dashv \delta^\uparrow \mathbf{T} \vdash \mathbf{180}_0^\uparrow \dashv \delta^\uparrow \mathbf{T} \vdash \mathbf{90}_\varphi^\uparrow$   |
|                        | $(\dagger) \mathbf{90}_{-\varphi}'^\uparrow \dashv \delta^\uparrow \mathbf{T} \vdash \mathbf{180}_0^\uparrow \dashv \delta^\uparrow \mathbf{T} \vdash \mathbf{90}_{-\varphi}^\uparrow$   |
| $\text{HMZ}(\varphi)$  | $\mathbf{90}_\varphi'^\uparrow \mathbf{180}_\pi'^\uparrow \mathbf{90}_\varphi'^\uparrow \dashv \delta^\uparrow \mathbf{T} \vdash \mathbf{180}_0^\uparrow \dashv \delta^\uparrow \mathbf{T} \vdash \mathbf{90}_{-\varphi}^\uparrow \mathbf{180}_\pi^\uparrow \mathbf{90}_{-\varphi}^\uparrow$ |
| $\text{HMZ}(-\varphi)$ | $\mathbf{90}_{-\varphi}'^\uparrow \mathbf{180}_\pi'^\uparrow \mathbf{90}_{-\varphi}'^\uparrow \dashv \delta^\uparrow \mathbf{T} \vdash \mathbf{180}_0^\uparrow \dashv \delta^\uparrow \mathbf{T} \vdash \mathbf{90}_\varphi^\uparrow \mathbf{180}_\pi^\uparrow \mathbf{90}_\varphi^\uparrow$ |

## B. HYPER MACH-ZEHNDER

We turn now to the atomic Mach-Zehnder (MZ) interferometer. Such a scheme is insensitive to constant clock detunings and Doppler-shifts making them accurate and sensitive inertial-force sensors [37, 58]. However, variations of the laser field amplitude during beam splitter action may restore a parasitic distortion related to a residual Doppler-shift [64]. So far, we consider wavepackets trajectories to be straight-lines to preserve the inherent symmetry of the MZ interferometer.

A composite pulse interferometer called hyper MZ

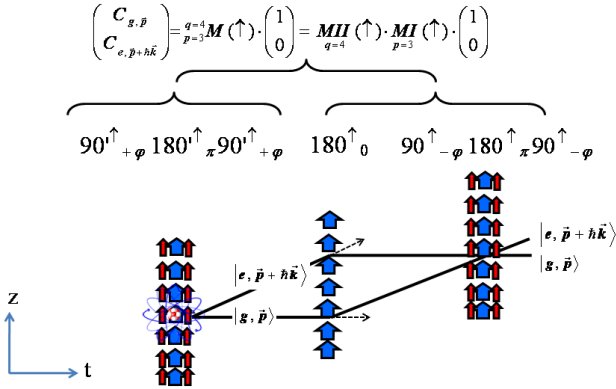


FIG. 9. (color online). (Left) Generalized hyper-Mach-Zehnder (HMZ) interferometer. Two sets of co-propagating composite laser pulses are separated by an intermediate  $\mathbf{180}_0^\uparrow$  pulse where  $\uparrow$  arrows are corresponding to laser detuning modified by  $kv_z$  Doppler wavevector orientation and atomic recoil (see Tab. III). The full interaction geometry can be directly evaluated either from a single interaction matrix  ${}_3^4\mathbf{M}(\uparrow)$  or from the product of two independent building-blocks  $\mathbf{MI}(\uparrow)$  and  $\mathbf{MII}(\uparrow)$  respectively with  $p = 3$  pulses and  $q = 4$  pulses. Laser pulse phases are chosen to be for the first set of pulses denoted as  $\varphi'_{1,3} = \varphi, \varphi'_2 = \pi$ , for the reverse pulse  $\varphi_1 = 0$  and  $\varphi_{2,4} = -\varphi, \varphi_3 = \pi$  for the last set of pulses.

(HMZ) is shown in Fig. 9. We propose to remove limits to the symmetry of the original MZ type under pulse area variation (see appendix, section S3 for analytical components needed to calculate the transition probability expression  $P_{\text{HMZ}}$ ). The first Ramsey  $\mathbf{90}_\varphi'^\uparrow$  pulse is replaced by a composite sequence  $\mathbf{90}_\varphi'^\uparrow \mathbf{180}_\pi'^\uparrow \mathbf{90}_\varphi'^\uparrow$  and the last Ramsey  $\mathbf{90}_0^\uparrow$  by the sequence  $\mathbf{90}_{-\varphi}^\uparrow \mathbf{180}_\pi^\uparrow \mathbf{90}_{-\varphi}^\uparrow$  with opposite phase-steps as reported in Tab. III.

The exact hyper Mach-Zehnder (HMZ) transition probability  $P_{\text{HMZ}}$  is now established fixing  $C_g(0) = 1, C_e(0) = 0$ . In such a configuration identical to the Hahn-echo scheme, the clock frequency dependence is removed [64]. The analytic computation can be still realized in two ways, reducing either the sequence of pulses to a single interaction matrix  ${}_3^4\mathbf{M}(\uparrow)$  or by decomposing the interaction geometry in a product of two independent building-blocks  $\mathbf{MI}(\uparrow)$  and  $\mathbf{MII}(\uparrow)$  respectively with  $p = 3$  pulses and  $q = 4$  pulses. In all cases, we take  $\delta^\uparrow \mathbf{T} \mapsto 0$  simplifying the calculation while the intermediate  $\mathbf{180}_0^\uparrow$  reverse pulse is now played by index  $l = 1$  in the second set of  $q$  pulses within the matrix  $\mathbf{MII}(\uparrow)$  (see Fig. 9).

Here, we employ some analytic results from appendix and section S3 used to evaluate the single interaction matrix  ${}_3^4\mathbf{M}(\uparrow)$  of the HMZ. The matter-wave interferometric signal is computed leading to the following expression:

$$P_{\text{HMZ}} = \left| {}_3^4\alpha_{gg} \left[ 1 - |{}_3^4\beta_{gg}| e^{-i{}_3^4\Phi(gg)} \right] \right|^2 \quad (27)$$

where  $\alpha_1'^3(gg), \alpha_1^4(gg) \mapsto \alpha_2^4(gg)$  and  $\beta_1'^3(gg), \beta_1^4(gg) \mapsto \beta_2^4(gg)$  (see appendix section S3 for laser index modification due to non overlapping wavepackets from the intermediate reversal pulse) are:

$$\begin{aligned} \alpha_1'^3(gg) &= \left( \prod_1^3 \cos \tilde{\vartheta}_l' e^{i\phi_l'} \right) \cdot (1 - S'_{3,2}) \\ S'_{3,2} &= e^{-i\Xi_{12}'} \tan \tilde{\vartheta}_1' \tan \tilde{\vartheta}_2' + e^{-i\Xi_{13}'} \tan \tilde{\vartheta}_1' \tan \tilde{\vartheta}_3' \\ &\quad + e^{-i\Xi_{23}'} \tan \tilde{\vartheta}_2' \tan \tilde{\vartheta}_3' \end{aligned} \quad (28)$$

and

$$\begin{aligned}\alpha_2^4(gg) &= \sin \tilde{\vartheta}_1 \left( \prod_2^{q=4} \cos \tilde{\vartheta}_l e^{i\phi_l} \right) \cdot (-S_{4,2} + S_{4,4}) \\ S_{4,2} &= e^{-i\Xi_{12}} \tan \tilde{\vartheta}_2 + e^{-i\Xi_{13}} \tan \tilde{\vartheta}_3 + e^{-i\Xi_{14}} \tan \tilde{\vartheta}_4 \\ S_{4,4} &= e^{-i\Xi_{1234}} \tan \tilde{\vartheta}_2 \tan \tilde{\vartheta}_3 \tan \tilde{\vartheta}_4\end{aligned}\quad (29)$$

with

$$\beta_1^3(gg) = \frac{\tan \tilde{\vartheta}'_1 + e^{-i\Xi'_{12}} \frac{\tan \tilde{\vartheta}'_2 + e^{-i\Xi'_{23}} \tan \tilde{\vartheta}'_3}{1 - e^{-i\Xi'_{23}} \tan \tilde{\vartheta}'_2 \tan \tilde{\vartheta}'_3}}{1 - e^{-i\Xi'_{12}} \tan \tilde{\vartheta}'_1 \frac{\tan \tilde{\vartheta}'_2 + e^{-i\Xi'_{23}} \tan \tilde{\vartheta}'_3}{1 - e^{-i\Xi'_{23}} \tan \tilde{\vartheta}'_2 \tan \tilde{\vartheta}'_3}} \quad (30a)$$

$$\beta_2^4(gg) = - \frac{1}{\frac{\tan \tilde{\vartheta}_2 + e^{-i\Xi_{23}} \frac{\tan \tilde{\vartheta}_3 + e^{-i\Xi_{34}} \tan \tilde{\vartheta}_4}{1 - e^{-i\Xi_{34}} \tan \tilde{\vartheta}_3 \tan \tilde{\vartheta}_4}}{1 - e^{-i\Xi_{23}} \tan \tilde{\vartheta}_2 \frac{\tan \tilde{\vartheta}_3 + e^{-i\Xi_{34}} \tan \tilde{\vartheta}_4}{1 - e^{-i\Xi_{34}} \tan \tilde{\vartheta}_3 \tan \tilde{\vartheta}_4}}} \quad (30b)$$

The HMZ composite phase-shift is:

$$\begin{aligned}{}_3^4\Phi(gg) &= -\varphi'_1 + 2\varphi_1 - \varphi_2 + \phi'_1 - \phi_2 \\ &\quad - (\text{Arg}[\beta_1^3(gg)] + \text{Arg}[\beta_2^4(gg)])\end{aligned}\quad (31)$$

However, a direct use of the HMZ phase-shift expression  ${}_3^4\Phi(gg)$  does not correspond to the correct evaluation of the true central fringe phase-shift. The transition probability given by Eq. 27 is a non-trivial spectral function, where the terms  $\alpha_1^3(gg)$ ,  $\alpha_2^4(gg)$  and  $\beta_1^3(gg)$ ,  $\beta_2^4(gg)$  depend on laser phases. For this reason, the composite phase-shift of the central fringe can not be easily associated to Eq. 31. The phase-shift related to the central interference is tracking numerically when fringes are recorded by scanning the laser phase  $\varphi$  of the HMZ composite pulse beam splitters.

As a validation of previous analytical calculations, we re-derive the original three-pulse MZ configuration with the intermediate  $180_0^\uparrow$  pulse still played with index  $l = 1$  in the second set of  $q$  pulses. We obtain, after straightforward simplification on envelops  $\alpha_1^3(gg)$ ,  $\alpha_2^4(gg)$  and complex terms  $\beta_1^3(gg)$ ,  $\beta_2^4(gg)$ , the MZ transition probability expressed as:

$$P_{\text{MZ}} = \left| -\cos \tilde{\vartheta}'_1 \sin \tilde{\vartheta}_1 \sin \tilde{\vartheta}_2 \cdot \left[ 1 + \frac{\tan \tilde{\vartheta}'_1}{\tan \tilde{\vartheta}_2} e^{-i\Phi(gg)} \right] \right|^2 \quad (32)$$

where, this time, the MZ phase-shift is easily identified to be:

$$\Phi(gg) = -\varphi'_1 + 2\varphi_1 - \varphi_2 + \phi'_1 - \phi_2 \quad (33)$$

consistent with [37, 38] when  $\phi'_1 = \phi_2$ . An additional MZ phase sensitivity to residual Doppler shifts is retrieved when  $\phi'_1 \neq \phi_2$  due to the imbalance of Rabi fields between the first and the last beam splitter pulse as expected [64]. We point out that a MZ interferometer is a particular

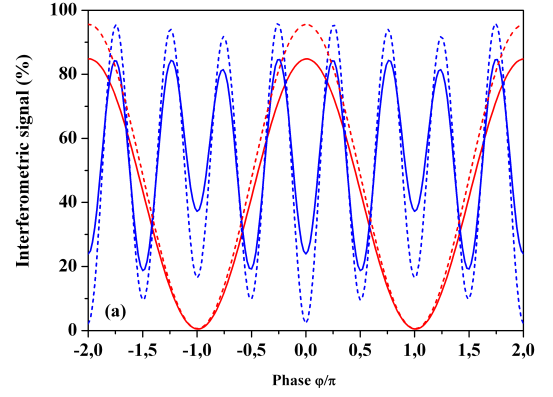


FIG. 10. (color online). (a) MZ (red) and HMZ (blue) matter-wave interferences versus scan of the laser phase  $\varphi$ . Solid lines are recorded with a residual Doppler-shift  $\delta_D/2\pi = 10\text{kHz}$  ( $\delta_D \equiv kv_z$ ) and dashed lines with  $\delta_D/2\pi = 5\text{kHz}$ . Pulse duration is  $\tau = 10\mu\text{s}$  and the Rabi frequency is  $\Omega = \pi/2\tau$ . A Rabi field error of 10% is fixed between the first beam splitter (or the first set of composite pulses) and the last one (or the last set of composite pulses) as in [64]. Note that the residual phase-shift induced by the pulse area error is too small to be seen on fringe minimum.

case of the symmetric RB configuration we have shortly discussed in the previous subsection. By fixing  $\varphi_1^I \equiv \varphi'_1$ ,  $\varphi_1^I = \varphi_1^{II} \equiv \varphi_1$ ,  $\varphi_1^I \equiv \varphi_2$  in Eq. 22a and  $\phi_1^I \equiv \phi'_1$ ,  $\phi_1^I = \phi_1^{II} \equiv \phi_1$  and  $\phi_1^I \equiv \phi_2$  in Eq. 22b, we retrieve the MZ phase-shift given by Eq. 33.

We have reported in Fig. 10 matter-wave interferences versus the laser phase of the beam splitters based on a three-pulse configuration (MZ with solid red and dashed lines) and using two sets of composite pulses (HMZ with solid blue and dashed lines). The laser phase is scanned only during the first (or the last) beam splitter of the three-pulse interferometer while all laser phases are simultaneously changed over the two sets of composite pulse beam splitters in the HMZ configuration. This results in a different inter-fringe between interferometers as shown in Fig. 10.

Several numerical plots of the center of fringes versus a residual Doppler shift  $\delta_D/2\pi$  ( $\delta_D \equiv kv_z$ ) is reported in Fig. 11(a) and (b) under a 10% pulse area error between the first beam splitter pulse (or the first set of composite pulses) and the last one (or the last set of composite pulses). The composite phase-shift generated by the HMZ scheme is highly nonlinear as it can be observed from Fig. 11(a). We remark that the phase-shift presents a divergence near a Doppler-shift  $\delta_D/2\pi \approx \pm 20\text{ kHz}$ . It is related to a sudden change from a minimum to a maximum of the fringe interference transition probability. The plots with red star from Fig. 11(a) corresponds to the MZ type interferometer exhibiting a dispersive phase-shift about 24 mrad for a Doppler-shift of 10 kHz in accordance with [64]. The plots with blue dots from Fig. 11(b) corresponds to the HMZ configuration with a non linear reduction of the phase-shift around 0.3 mrad for the same

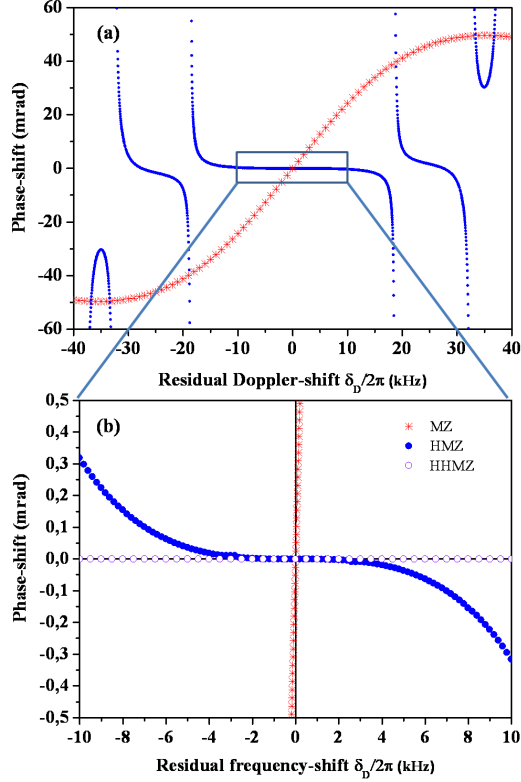


FIG. 11. (color online). (a) Numerical tracking of the central interference position versus a residual Doppler-shift  $\delta_D/2\pi$  for MZ interferometer ( $\star$  red stars) and HMZ ( $\bullet$  blue dots). (b) Zoom of the central interference position versus  $\delta_D/2\pi$  including the additional hybrid HHMZ scheme ( $\circ$  violet open dots).

Doppler-shift. Following error signal generation based on Eq. 9, a new set of plots with open circles in Fig. 11(b) are produced by an hybrid combination of HMZ interferometric signals (HHMZ) with opposite phase-steps as (see the last protocol from Tab. III):

$$P_{\text{HHMZ}} = \frac{P_{\text{HMZ}}(\varphi) + P_{\text{HMZ}}(-\varphi)}{2} \quad (34)$$

Such a combination of signals is again cooperatively adding interference fringes with opposite phase-shifts to completely cancel the residual correction [69]. The HMZ interferometer is demonstrated to be more robust against velocity-distribution asymmetries activated by pulse area error that may lead to parasitic shifts compromising the accuracy. We have also verified that an additional contribution from any uncompensated asymmetric light-shifts of a few % between sets of composite pulses are still strongly reduced to the same level of correction [65].

## V. CONCLUSIONS AND OUTLOOK

We have explored new applications of composite pulses from optical clocks to Ramsey-Bordé and Mach-Zehnder atom interferometers, and demonstrate that they might be designed to be more robust against pulse defects related to laser field amplitude variation coupled to residual Doppler-shifts and light-shifts between multiple interaction zones. We have introduced a new set of composite atomic beam-splitters with concatenated pulses tailored in frequency, duration and phase-steps to efficiently mitigate laser induced phase-shift distortions on optical Ramsey interferences.

The limits of actual atomic interferometry experiments raise the important question about inhomogeneities of phases and amplitudes of laser pulses used to diffract matter-waves related to the size of the atomic ensemble which is thermally expanding over time. Among these effects that have important consequences, the recoil determination can be modified in a distorted optical field [70] and intensity-dependent phase-shifts are present through distortions in the wavefronts of the Bragg beams [71]. These error sources driven by fluctuation of coherent light excitation might be minimized by active control of laser wavefront [72] and using colder atomic sources [73, 74]. For example, some of these systematics have been reduced through a spatial-filtering process by controlling the detection volume and limiting the spatial extent of the atom cloud before the interrogation protocol [71].

Hyper Ramsey-Bordé matter-wave interferometry is primarily dedicated to a new class of atomic interferometers using long-lived optical clock transitions in fermionic and bosonic alkaline-earth species inducing large momentum transfer [75–77] but suffering from systematics coupled to undesirable ac Stark-shifts and magnetic-shift instabilities [78–83]. Advancing atomic and molecular coherent matter-wave manipulation with the latest laser pulse techniques from clock interferometry [84, 85] will bring atomic sensors to robust real-world application [86] from portable optical clocks to mobile gravimeters [87–91] as well as boosting performances of actual devices with a minimal experimental effort. Combining such sensors with very recent quantum technologies through entanglement and spin squeezing [92–94] will improve high-precision laser spectroscopy and metrology below a relative level of  $10^{-19}$  in accuracy, opening new applications to track gravity induced phase-shifts in Ramsey interferometry [95] or to detect gravitational waves in a frequency band between the LISA and LIGO detectors [77, 96–99] while searching for new fundamental physics behind the standard model with a better accuracy [100].

## ACKNOWLEDGMENTS

T.Z.W deeply thanks F. Pereira dos Santos and M. Cadoret for constructive comments about atomic interferometry, M. Glass-Maujean for a careful reading of the

manuscript and J. Ye for exciting discussion. I would here express a very deep acknowledgement to C.J. Bordé for interest in this work. V.I.Yudin was supported by the Russian Foundation for Basic Research (Grant Nos. 20-02-00505 and 19-32-90181) and Foundation for the Advancement of Theoretical Physics and Mathematics "BASIS". A.V. Taichenachev acknowledges financial support from Russian Science Foundation through the grant 20-12-00081. T.Z.W. also acknowledges Sorbonne Université for a six months CRCT (Congés pour Recherches ou Conversions Thématiques) and MajuLab, CNRS-UCA-SU-NUS-NTU for supporting a six months collaborative project.

## APPENDIX

We turn to look for an exact expression of the interaction matrix  ${}^qM$  using  $p, q$  pulses applied around a single free evolution time. We present our computational algorithm establishing matrix components  ${}^qC_{gg}, {}^qC_{ge}$  required to compute the transition probability generalizing the previous work by [40].

### S0: SYMMETRIC FUNCTIONS $S'_{p,k}$ AND $S_{q,k}$

We derive formulae and phase association rules to evaluate envelop terms  $\alpha_l^p(gg)$ ,  $\alpha_l^q(gg)$  and  $\alpha_l^p(ge)$  using some notations from [45] as following:

$$\alpha_l^p(gg) = \left( \prod_{l=1}^p \cos \tilde{\vartheta}_l e^{i\phi_l'} \right) \cdot \left( \sum_{\text{even } k \geq 0} (-1)^{\frac{k}{2}} S'_{p,k}(gg) \right) \quad (35a)$$

$$\alpha_l^q(gg) = \left( \prod_{l=1}^q \cos \tilde{\vartheta}_l e^{i\phi_l} \right) \cdot \left( \sum_{\text{even } k \geq 0} (-1)^{\frac{k}{2}} S_{q,k}(gg) \right) \quad (35b)$$

$$\alpha_l^p(ge) = \tilde{\alpha}' \left( \prod_{l=1}^p \cos \tilde{\vartheta}_l e^{i\phi_l'} \right) \cdot \left( \sum_{\text{odd } k \geq 1} (-1)^{\frac{k-1}{2}} S'_{p,k}(ge) \right) \quad (35c)$$

with  $\tilde{\alpha}' = -ie^{-i(\phi_p' + \varphi_p' + \Xi_p')}$  in Eq. 35c. The convention is  $S'_{p,0} = S_{q,0} = 1$  in Eq. 35a and Eq. 35b. Symmetric functions  $S'_{p,k}$  and  $S_{q,k}$  having respectively  $\frac{p!}{k!(p-k)!}$  and

$\frac{q!}{k!(q-k)!}$  elements are:

$$S'_{p,k}(gg) = \sum_{\substack{A \subseteq \{1, 2, 3, \dots, p\} \\ |A| = k}} e^{-i\Xi'_A} \prod_{l \in A} \tan \tilde{\vartheta}_l' \quad (36a)$$

$$S_{q,k}(gg) = \sum_{\substack{A \subseteq \{1, 2, 3, \dots, p\} \\ |A| = k}} e^{-i\Xi_A} \prod_{l \in A} \tan \tilde{\vartheta}_l \quad (36b)$$

$$S'_{p,k}(ge) = \sum_{\substack{A \subseteq \{1, 2, 3, \dots, p\} \\ |A| = k}} e^{i\Xi'_A} \prod_{l \in A} \tan \tilde{\vartheta}_l' \quad (36c)$$

Note that phase factors  $\Xi'_A$  as well as  $\Xi_A$  that are affected to the product in Eq. 36a and Eq. 36b are determined by all possible k-combination of l elements in A ensemble with k even. The decomposition rules of  $\Xi'_A$  ( $\Xi_A$ ) are presented: for  $|A| = 2$ , phase-factors are given by  $\Xi'_A \equiv \Xi'_{12}, \Xi'_{23}, \dots, \Xi'_{13}, \Xi'_{24}, \dots$  where the decomposition is  $\Xi'_{13} = \Xi'_{12} + \Xi'_{23}, \dots$ . For  $|A| = 4$ , we get  $\Xi'_A \equiv \Xi'_{1234}, \Xi'_{2345}, \dots, \Xi'_{1345}, \dots$  where  $\Xi'_{1234} = \Xi'_{12} + \Xi'_{34}, \dots$  and so on.

Phase factors  $\Xi'_A$  affected to the product in Eq. 36c are determined by all possible k-combination of l elements in A ensemble with k odd. For  $|A| = 1$ , phase-factors are given by  $\Xi'_A \equiv \Xi'_1, \Xi'_2, \Xi'_3, \dots$ . Here, by convention  $\Xi'_1 = 0$  and  $\Xi'_2 \equiv \Xi'_{12}, \Xi'_3 \equiv \Xi'_{13}, \dots$  where the decomposition is  $\Xi'_{12} = \Xi'_{12}, \Xi'_{13} = \Xi'_{12} + \Xi'_{23}, \Xi'_{14} = \Xi'_{12} + \Xi'_{23} + \Xi'_{34}, \dots$ . For  $|A| = 3$ , we get  $\Xi'_A \equiv \Xi'_{123}, \Xi'_{124}, \Xi'_{134}, \dots, \Xi'_{234}, \dots$  where  $\Xi'_{123} = \Xi'_1 + \Xi'_{23}, \Xi'_{124} = \Xi'_1 + \Xi'_{24}, \dots, \Xi'_{234} = \Xi'_2 + \Xi'_{34}, \dots$  and so on. The basic structure of all phase-factors is  $\Xi'_{l,l+1} = \varphi'_l - \varphi'_{l+1} + \phi'_l + \phi'_{l+1}$  for  $\Xi'_A$  and  $\Xi_{l,l+1} = \varphi_{l+1} - \varphi_l + \phi_l + \phi_{l+1}$  for  $\Xi_A$ .

### S1: SPINOR COMPONENTS WITH $p = q = 4$

We present an interaction matrix  ${}^4M$  based on four pulses. The matrix components  ${}^4C_{gg}, {}^4C_{ge}$  we need to evaluate are evaluated by the following elements:

$$\alpha_1^{I4}(gg) = \left( \prod_1^{p=4} \cos \tilde{\vartheta}_l' e^{i\phi_l'} \right) \cdot (1 - S'_{4,2} + S'_{4,4}) \quad (37a)$$

$$\alpha_1^4(gg) = \left( \prod_1^{q=4} \cos \tilde{\vartheta}_l e^{i\phi_l} \right) \cdot (1 - S_{4,2} + S_{4,4}) \quad (37b)$$

$$\alpha_1^{I4}(ge) = -ie^{-i(\phi_4' + \varphi_4' + \Xi_4')} \quad (37c)$$

$$\times \left( \prod_1^{p=4} \cos \tilde{\vartheta}_l' e^{i\phi_l'} \right) \cdot (S'_{4,1} - S'_{4,3}) \quad (37d)$$



We have for  $S'_{4,k}(gg)$ :

$$\begin{aligned}
S'_{4,0} &= 1 \\
S'_{4,2} &= e^{-i\Xi'_{12}} \tan \tilde{\vartheta}'_1 \tan \tilde{\vartheta}'_2 + e^{-i\Xi'_{23}} \tan \tilde{\vartheta}'_2 \tan \tilde{\vartheta}'_3 \\
&\quad + e^{-i\Xi'_{34}} \tan \tilde{\vartheta}'_3 \tan \tilde{\vartheta}'_4 + e^{-i\Xi'_{13}} \tan \tilde{\vartheta}'_1 \tan \tilde{\vartheta}'_3 \\
&\quad + e^{-i\Xi'_{14}} \tan \tilde{\vartheta}'_1 \tan \tilde{\vartheta}'_4 \\
S'_{4,4} &= e^{-i\Xi'_{1234}} \tan \tilde{\vartheta}'_1 \tan \tilde{\vartheta}'_2 \tan \tilde{\vartheta}'_3 \tan \tilde{\vartheta}'_4
\end{aligned} \tag{38}$$

and for  $S'_{4,k}(ge)$ :

$$\begin{aligned}
S'_{4,1} &= \tan \tilde{\vartheta}'_1 + e^{i\Xi'_2} \tan \tilde{\vartheta}'_2 \\
&\quad + e^{i\Xi'_3} \tan \tilde{\vartheta}'_3 + e^{i\Xi'_4} \tan \tilde{\vartheta}'_4 \\
S'_{4,3} &= e^{i\Xi'_{123}} \tan \tilde{\vartheta}'_1 \tan \tilde{\vartheta}'_2 \tan \tilde{\vartheta}'_3 \\
&\quad + e^{i\Xi'_{124}} \tan \tilde{\vartheta}'_1 \tan \tilde{\vartheta}'_2 \tan \tilde{\vartheta}'_4 \\
&\quad + e^{i\Xi'_{134}} \tan \tilde{\vartheta}'_1 \tan \tilde{\vartheta}'_3 \tan \tilde{\vartheta}'_4 \\
&\quad + e^{i\Xi'_{234}} \tan \tilde{\vartheta}'_2 \tan \tilde{\vartheta}'_3 \tan \tilde{\vartheta}'_4
\end{aligned} \tag{39}$$

We also have for  $S_{4,k}(gg)$  elements:

$$\begin{aligned}
S_{4,0} &= 1 \\
S_{4,2} &= e^{-i\Xi_{12}} \tan \tilde{\vartheta}_1 \tan \tilde{\vartheta}_2 + e^{-i\Xi_{23}} \tan \tilde{\vartheta}_2 \tan \tilde{\vartheta}_3 \\
&\quad + e^{-i\Xi_{34}} \tan \tilde{\vartheta}_3 \tan \tilde{\vartheta}_4 + e^{-i\Xi_{13}} \tan \tilde{\vartheta}_1 \tan \tilde{\vartheta}_3 \\
&\quad + e^{-i\Xi_{14}} \tan \tilde{\vartheta}_1 \tan \tilde{\vartheta}_4 + e^{-i\Xi_{24}} \tan \tilde{\vartheta}_2 \tan \tilde{\vartheta}_4 \\
S_{4,4} &= e^{-i\Xi_{1234}} \tan \tilde{\vartheta}_1 \tan \tilde{\vartheta}_2 \tan \tilde{\vartheta}_3 \tan \tilde{\vartheta}_4
\end{aligned} \tag{40}$$

The corresponding complex phase factor  $\beta_1'^4(gg), \beta_1^4(gg)$  leading to a phase-shift correction are now:

$$\begin{aligned}
\beta_1'^4(gg) &= \frac{\tan \tilde{\vartheta}'_1 + e^{-i\Xi'_{12}} \frac{\tan \tilde{\vartheta}'_2 + e^{-i\Xi'_{23}} \frac{\tan \tilde{\vartheta}'_3 + e^{-i\Xi'_{34}} \tan \tilde{\vartheta}'_4}{1 - e^{-i\Xi'_{34}} \tan \tilde{\vartheta}'_3 \tan \tilde{\vartheta}'_4}}{1 - e^{-i\Xi'_{23}} \tan \tilde{\vartheta}'_2} \frac{\tan \tilde{\vartheta}'_3 + e^{-i\Xi'_{34}} \tan \tilde{\vartheta}'_4}{1 - e^{-i\Xi'_{34}} \tan \tilde{\vartheta}'_3 \tan \tilde{\vartheta}'_4}}{1 - e^{-i\Xi'_{12}} \tan \tilde{\vartheta}'_1} \frac{\tan \tilde{\vartheta}'_2 + e^{-i\Xi'_{23}} \frac{\tan \tilde{\vartheta}'_3 + e^{-i\Xi'_{34}} \tan \tilde{\vartheta}'_4}{1 - e^{-i\Xi'_{34}} \tan \tilde{\vartheta}'_3 \tan \tilde{\vartheta}'_4}}{1 - e^{-i\Xi'_{23}} \tan \tilde{\vartheta}'_2} \frac{\tan \tilde{\vartheta}'_3 + e^{-i\Xi'_{34}} \tan \tilde{\vartheta}'_4}{1 - e^{-i\Xi'_{34}} \tan \tilde{\vartheta}'_3 \tan \tilde{\vartheta}'_4}} \\
&\tag{41a}
\end{aligned}$$

$$\begin{aligned}
\beta_1^4(gg) &= \frac{\tan \tilde{\vartheta}_1 + e^{-i\Xi_{12}} \frac{\tan \tilde{\vartheta}_2 + e^{-i\Xi_{23}} \frac{\tan \tilde{\vartheta}_3 + e^{-i\Xi_{34}} \tan \tilde{\vartheta}_4}{1 - e^{-i\Xi_{34}} \tan \tilde{\vartheta}_3 \tan \tilde{\vartheta}_4}}{1 - e^{-i\Xi_{23}} \tan \tilde{\vartheta}_2} \frac{\tan \tilde{\vartheta}_3 + e^{-i\Xi_{34}} \tan \tilde{\vartheta}_4}{1 - e^{-i\Xi_{34}} \tan \tilde{\vartheta}_3 \tan \tilde{\vartheta}_4}}{1 - e^{-i\Xi_{12}} \tan \tilde{\vartheta}_1} \frac{\tan \tilde{\vartheta}_2 + e^{-i\Xi_{23}} \frac{\tan \tilde{\vartheta}_3 + e^{-i\Xi_{34}} \tan \tilde{\vartheta}_4}{1 - e^{-i\Xi_{34}} \tan \tilde{\vartheta}_3 \tan \tilde{\vartheta}_4}}{1 - e^{-i\Xi_{23}} \tan \tilde{\vartheta}_2} \frac{\tan \tilde{\vartheta}_3 + e^{-i\Xi_{34}} \tan \tilde{\vartheta}_4}{1 - e^{-i\Xi_{34}} \tan \tilde{\vartheta}_3 \tan \tilde{\vartheta}_4}} \\
&\tag{41b}
\end{aligned}$$

$$\beta_1'^4(ge) = \frac{1}{\{\beta_1'^4(gg)\}^*} \tag{41c}$$

We give the decomposition of phase factor expressions as following:

$$\begin{aligned}
\Xi'_1 &= 0 \\
\Xi'_2 &= \Xi'_{12} \\
\Xi'_3 &= \Xi'_{13} \\
\Xi'_4 &= \Xi'_{14} \\
\Xi'_{123} &= \Xi'_1 + \Xi'_{23} \\
\Xi'_{124} &= \Xi'_1 + \Xi'_{24} \\
\Xi'_{134} &= \Xi'_1 + \Xi'_{34} \\
\Xi'_{234} &= \Xi'_2 + \Xi'_{34}
\end{aligned} \tag{42}$$

$$\begin{aligned}
\Xi'_{12} &= \varphi'_1 - \varphi'_2 + \phi'_1 + \phi'_2 \\
\Xi'_{23} &= \varphi'_2 - \varphi'_3 + \phi'_2 + \phi'_3 \\
\Xi'_{34} &= \varphi'_3 - \varphi'_4 + \phi'_3 + \phi'_4 \\
\Xi'_{13} &= \Xi'_{12} + \Xi'_{23} \\
\Xi'_{24} &= \Xi'_{23} + \Xi'_{34} \\
\Xi'_{14} &= \Xi'_{12} + \Xi'_{23} + \Xi'_{34} \\
\Xi'_{1234} &= \Xi'_{12} + \Xi'_{34}
\end{aligned} \tag{43}$$

and:

$$\begin{aligned}
\Xi_{12} &= \varphi_2 - \varphi_1 + \phi_1 + \phi_2 \\
\Xi_{23} &= \varphi_3 - \varphi_2 + \phi_2 + \phi_3 \\
\Xi_{34} &= \varphi_4 - \varphi_3 + \phi_3 + \phi_4 \\
\Xi_{13} &= \Xi_{12} + \Xi_{23} \\
\Xi_{24} &= \Xi_{23} + \Xi_{34} \\
\Xi_{14} &= \Xi_{12} + \Xi_{23} + \Xi_{34} \\
\Xi_{1234} &= \Xi_{12} + \Xi_{34}
\end{aligned} \tag{44}$$

See also [50] as another way to obtain  ${}^4C_{ge}$  from  ${}^4C_{gg}$ .

## S2: GHRB COMPONENTS WITH $p = 1, q = 2$

For a general purpose, we explicitly give interaction matrix components  ${}^2_1\mathbf{MI}(\uparrow)(\downarrow)$  and  ${}^2_1\mathbf{MI}(\downarrow)(\uparrow)$  inside successive building-blocks that are including pairs of traveling waves with opposite orientation to close the interferometer. We have for the first  ${}^2_1\mathbf{MI}(\uparrow)(\downarrow)$  interaction zone, the following components:

$$\begin{aligned}
{}^2_1\alpha_{gg}^I &= \alpha_1'^{1I}(gg) \cdot \alpha_1^{2I}(gg) \\
{}^2_1\alpha_{ge}^I &= \alpha_1'^{1I}(ge) \cdot \alpha_1^{2I}(gg) \\
{}^2_1\beta_{gg}^I &= \beta_1'^{1I}(gg) \cdot \beta_1^{2I}(gg) \\
{}^2_1\beta_{ge}^I &= \beta_1'^{1I}(ge) \cdot \beta_1^{2I}(gg)
\end{aligned} \tag{45}$$

where we have:

$$\begin{aligned}
\alpha_1'^{1I}(gg) &= \cos \tilde{\vartheta}'_1 e^{i\phi'_1} \\
\alpha_1^{2I}(gg) &= \cos \tilde{\vartheta}_1 \cos \tilde{\vartheta}_2 e^{i(\phi_1 + \phi_2)} \cdot (1 - S_{2,2}) \\
\beta_1'^{1I}(gg) &= \tan \tilde{\vartheta}'_1 \\
\beta_1^{2I}(gg) &= \frac{\tan \tilde{\vartheta}_1 + e^{-i\Xi_{12}} \tan \tilde{\vartheta}_2}{1 - e^{-i\Xi_{12}} \tan \tilde{\vartheta}_1 \tan \tilde{\vartheta}_2}
\end{aligned} \tag{46}$$

and

$$\begin{aligned}\alpha_1'^{1I}(ge) &= -i \sin \tilde{\vartheta}_1' e^{-i(\varphi_1' + \phi_1')} e^{i\phi_1'} \\ \beta_1'^{1I}(ge) &= \frac{1}{\tan \tilde{\vartheta}_1'}\end{aligned}\quad (47)$$

with a laser detuning definition given by  $\delta_I^{\uparrow\downarrow} = \delta \mp kv_z - \delta_r + \Delta_I$  for wavevector orientation.

We have for the second  ${}^2\text{MII}(\downarrow)(\uparrow)$  interaction zone with opposite wavevectors the following components:

$$\begin{aligned}{}^2_1\alpha_{gg}^{II} &= \alpha_1'^{1II}(gg) \cdot \alpha_1'^{2II}(gg) \\ {}^2_1\alpha_{ge}^{II} &= \alpha_1'^{1II}(ge) \cdot \alpha_1'^{2II}(gg) \\ {}^2_1\beta_{gg}^{II} &= \beta_1'^{1II}(gg) \cdot \beta_1'^{2II}(gg) \\ {}^2_1\beta_{ge}^{II} &= \beta_1'^{1II}(ge) \cdot \beta_1'^{2II}(gg)\end{aligned}\quad (48)$$

where laser detunings are given by  $\delta_{II}^{\uparrow\downarrow} = \delta \pm kv_z + 3\delta_r + \Delta_{II}$  for the down-shifted frequency component and  $\delta_{II}^{\uparrow\downarrow} = \delta \pm kv_z - \delta_r + \Delta_{II}$  for the up-shifted component by the atomic recoil.

We have used definitions from [41, 42] for arbitrary transverse Doppler-shift orientation and momentum quantization along each path of the interferometer.

### S3: HMZ COMPONENTS WITH $p = 3, q = 4$

Some analytic results from section S1 are used again to evaluate a single interaction matrix  ${}^4_3\text{M}(\uparrow)$  including a composite set of  $p = 3$  pulses for the left side of the HMZ ( $\text{MI}(\uparrow)$ ) and a composite set of  $q = 4$  pulses for the right side of the HMZ ( $\text{MII}(\uparrow)$ ). The matter-wave interferometric signal can be thus directly computed leading to the complex expression:

$$P_{\text{HMZ}} = \left| {}^4_3\alpha_{gg} \left[ 1 - |{}^4_3\beta_{gg}| e^{-i{}^4_3\Phi(gg)} \right] \right|^2 \quad (49)$$

where

$${}^4_3\alpha_{gg} = \alpha_1'^3(gg) \cdot \alpha_1'^4(gg) \quad (50a)$$

$${}^4_3\beta_{gg} = \beta_1'^3(gg) \cdot \beta_1'^4(gg) \quad (50b)$$

with

$$\alpha_1'^3(gg) = \left( \prod_1^3 \cos \tilde{\vartheta}_l' e^{i\phi_1'} \right) \cdot (1 - S'_{3,2}) \quad (51a)$$

$$\alpha_1'^4(gg) = \left( \prod_1^{q=4} \cos \tilde{\vartheta}_l' e^{i\phi_1'} \right) \cdot (1 - S_{4,2} + S_{4,4}) \quad (51b)$$

and

$$\beta_1'^3(gg) = \frac{\tan \tilde{\vartheta}_1' + e^{-i\Xi_{12}'} \frac{\tan \tilde{\vartheta}_2' + e^{-i\Xi_{23}'} \tan \tilde{\vartheta}_3'}{1 - e^{-i\Xi_{23}'} \tan \tilde{\vartheta}_2' \tan \tilde{\vartheta}_3'}}}{1 - e^{-i\Xi_{12}'} \tan \tilde{\vartheta}_1' \frac{\tan \tilde{\vartheta}_2' + e^{-i\Xi_{23}'} \tan \tilde{\vartheta}_3'}{1 - e^{-i\Xi_{23}'} \tan \tilde{\vartheta}_2' \tan \tilde{\vartheta}_3'}}} \quad (52a)$$

$$\beta_1'^4(gg) = \frac{\tan \tilde{\vartheta}_1' + e^{-i\Xi_{12}'} \frac{\tan \tilde{\vartheta}_2' + e^{-i\Xi_{23}'} \frac{\tan \tilde{\vartheta}_3' + e^{-i\Xi_{34}'} \tan \tilde{\vartheta}_4'}{1 - e^{-i\Xi_{34}'} \tan \tilde{\vartheta}_3' \tan \tilde{\vartheta}_4'}}}{1 - e^{-i\Xi_{23}'} \tan \tilde{\vartheta}_2' \frac{\tan \tilde{\vartheta}_3' + e^{-i\Xi_{34}'} \tan \tilde{\vartheta}_4'}{1 - e^{-i\Xi_{34}'} \tan \tilde{\vartheta}_3' \tan \tilde{\vartheta}_4'}}}}{1 - e^{-i\Xi_{12}'} \tan \tilde{\vartheta}_1' \frac{\tan \tilde{\vartheta}_2' + e^{-i\Xi_{23}'} \frac{\tan \tilde{\vartheta}_3' + e^{-i\Xi_{34}'} \tan \tilde{\vartheta}_4'}{1 - e^{-i\Xi_{34}'} \tan \tilde{\vartheta}_3' \tan \tilde{\vartheta}_4'}}}{1 - e^{-i\Xi_{23}'} \tan \tilde{\vartheta}_2' \frac{\tan \tilde{\vartheta}_3' + e^{-i\Xi_{34}'} \tan \tilde{\vartheta}_4'}{1 - e^{-i\Xi_{34}'} \tan \tilde{\vartheta}_3' \tan \tilde{\vartheta}_4'}}}} \quad (52b)$$

We now apply  $\cos \tilde{\vartheta}_1 e^{i\phi_1} \mapsto 0$  with  $\phi_1 = 0$  while keeping  $\sin \tilde{\vartheta}_1$  in Eq.51b and Eq.52b. It takes into account non-overlapping matter-waves during the intermediate  $180_0^\uparrow$  action. We finally get modified expressions for  $\alpha_1^4(gg) \mapsto \alpha_2^4(gg)$  and  $\beta_1^4(gg) \mapsto \beta_2^4(gg)$  within section IV.B of the main text.

- 
- [1] N.F. Ramsey, *A Molecular Beam Resonance Method with Separated Oscillating Fields*, *Phys. Rev.* **78**, 695 (1950).
  - [2] N.F. Ramsey and H.B. Silsbee, *Phase Shifts in the Molecular Beam Method of Separated Oscillating Fields*, *Phys. Rev.* **84**, 506 (1951).
  - [3] N.F. Ramsey, *Molecular Beams*, Oxford University Press, Oxford, (1956).
  - [4] N.F. Ramsey, *Molecular Beam Resonances in Oscillatory Fields of Nonuniform Amplitudes and Phases*, *Phys. Rev.* **109**, 822 (1958).
  - [5] M. Abgrall *et al.*, *Atomic fountains and optical clocks at SYRTE: Status and perspectives*, *C. R. Physique* **16**, 461 (2015).
  - [6] C.J Bordé, *Atomic interferometry with internal state labelling*, *Phys. Lett. A* **140**, 10, (1989).
  - [7] C.J Bordé, *Atomic clocks and inertial sensors*, *Metrologia* **39**, 435, (2002).
  - [8] C.J Bordé, *From first carbon dioxide lasers to atomic and molecular interferometers*, *C. R. Physique* **20**, 682, (2019).
  - [9] B.Ya. Dubetsky, A.P. Kazantsev, V.P. Chebotayev and V.P. Yakovlev, *Interference of atoms and formation of atomic spatial arrays in light fields*, *Pis'ma Eksp. Teor. Fiz.* **39**, 531, (1984), *JETP letters* **39**, 649, (1984).
  - [10] V.P. Chebotayev, B.Ya. Dubetsky, A.P. Kazantsev and V.P. Yakovlev, *Interference of atoms in separated optical fields*, *J. Opt. Soc. Am. B* **2**, 1791, (1985).
  - [11] F. Riehle, Th. Kisters, A. Witte, J. Helmcke and Ch.J. Bordé, *Optical Ramsey spectroscopy in a rotating frame: Sagnac effect in a matter-wave interferometer*, *Phys. Rev. Lett.* **67**, 177 (1991).

- [12] T.L. Gustavson, A. Landragin and M.A. Kasevich, *Rotation sensing with a dual atom-interferometer Sagnac gyroscope*, *Class. Quantum Grav.* **17**, 2385 (2000).
- [13] M. Kasevich and S. Chu, *Measurement of the gravitational acceleration of an atom with a light-pulse atom interferometer*, *Appl. Phys. B* **54**, 321 (1992).
- [14] D.S. Weiss, B.C. Young and S. Chu, *Precision measurement of the photon recoil of an atom using atomic interferometry*, *Phys. Rev. Lett.* **70**, 2706 (1993).
- [15] D.S. Weiss, B.C. Young and S. Chu, *Precision measurement of  $\hbar/m_Cs$  based on photon recoil using laser-cooled atoms and atomic interferometry*, *Appl. Phys. B* **59**, 217 (1994).
- [16] R. Bouchendira, P. Cladé, S. Guellati-Khélifa, F. Nez and F. Biraben, *New Determination of the Fine Structure Constant and Test of the Quantum Electrodynamics*, *Phys. Rev. Lett.* **106**, 080801 (2011).
- [17] R.H. Parker, C. Yu, W. Zhong, B. Estey and H. Müller, *Measurement of the fine-structure constant as a test of the Standard Model*, *Science* **360**, 191 (2018).
- [18] P. Cladé, F. Nez, F. Biraben and S. Guellati-Khelifa, *State of the art in the determination of the fine-structure constant and the ratio  $\hbar/m_u$* , *C. R. Physique* **20**, 77, (2019).
- [19] L. Morel, Z. Yao, P. Cladé, S. Guellati-Khélifa, *Determination of the fine-structure constant with an accuracy of 81 parts per trillion*, *Nature* **588**, 61, (2020).
- [20] J. Olson, R.W. Fox, T.M. Fortier, T.F. Sheerin, R.C. Brown, H. Leopardi, R.E. Stoner, C.W. Oates and A.D. Ludlow, *Ramsey-Bordé Matter-Wave Interferometry for Laser Frequency Stabilization at  $10^{-16}$  Frequency Instability and Below*, *Phys. Rev. Lett.* **123**, 073202 (2019).
- [21] A. Peters, K. Yeow Chung and S. Chu, *Measurement of gravitational acceleration by dropping atoms*, *Nature* **400**, 849 (1999).
- [22] G. Rosi, F. Sorrentino, L. Cacciapuoti, M. Prevedelli and G.M. Tino, *Precision measurement of the Newtonian gravitational constant using cold atoms*, *Nature* **510**, 518 (2014).
- [23] P. Asenbaum, C. Overstreet, M. Kim, J. Curti and M.A. Kasevich, *Atom-interferometric test of the equivalence principle at the  $10^{-12}$  level*, *Phys. Rev. Lett.* **125**, 191101 (2020).
- [24] M.H. Levitt, *Composite pulses*, *Prog. Nucl. Mag. Res. Spect.* **18**, 61 (1986).
- [25] S. Wimpey, *Broadband, narrowband, and passband composite pulses for use in advanced NMR experiments*, *J. Magn. Reson. Ser. A* **109**, 221 (1994).
- [26] L.M.K. Vandersypen and I.L. Chuang, *NMR techniques for quantum control and computation*, *Rev. Mod. Phys.* **76**, 1037 (2004).
- [27] J.A. Jones, *Quantum computing with NMR*, *Prog. Nucl. Mag. Res. Spect.* **59**, 91 (2011).
- [28] J. True Merrill and K.R. Brown, *Progress in compensating pulse sequences for quantum computation*, *Advan. Chem. Phys.* **154**, 241 (2014).
- [29] J.C. Saywell, I. Kuprov, D. Goodwin, M. Carey and T. Freegarde, *Optimal control of mirror pulses for cold-atom interferometry*, *Phys. Rev. A* **98**, 023625 (2018).
- [30] J. Saywell, M. Carey, M. Belal, I. Kuprov and T. Freegarde, *Optimal control of Raman pulse sequences for atom interferometry*, *J. Phys. B: At. Mol. Opt. Phys.* **53**, 085006 (2020).
- [31] G.A. Olivares-Renteria, D.A. Lancheros-Naranjo, E. Gomez and J.A. Franco-Villafañe, *Quantum gravimetry in the same internal state using composite light Raman pulses*, *Phys. Rev. A* **101**, 043613 (2020).
- [32] V.I. Yudin, A.V. Taichenachev, C.W. Oates, Z.W. Barber, N.D. Lemke, A.D. Ludlow, U. Sterr, Ch. Lisdat and F. Riehle, *Hyper-Ramsey spectroscopy of optical clock transitions*, *Phys. Rev. A* **82**, 011804(R) (2010).
- [33] N. Huntemann, B. Lipphardt, M. Okhapkin, Chr. Tamm, E. Peik, A.V. Taichenachev and V.I. Yudin, *Generalized Ramsey Excitation Scheme with Suppressed Light Shift*, *Phys. Rev. Lett.* **109**, 213002 (2012).
- [34] T. Zanon-Willette, V.I. Yudin, and A.V. Taichenachev, *Generalized hyper-Ramsey resonance with separated oscillating fields*, *Phys. Rev. A* **92**, 023416 (2015).
- [35] T. Zanon-Willette, R. Lefevre, A.V. Taichenachev and V.I. Yudin, *Universal interrogation protocol with zero probe-field-induced frequency shift for quantum clocks and high-accuracy spectroscopy*, *Phys. Rev. A* **96**, 023408 (2017).
- [36] T. Zanon-Willette, R. Lefevre, R. Metzдорff, N. Sillitoe, S. Almonacil, M. Minissale, E. de Clercq, A.V. Taichenachev, V.I. Yudin and E. Arimondo, *Composite laser-pulses spectroscopy for high-accuracy optical clocks: a review of recent progress and perspectives*, *Rep. Prog. Phys.* **81**, 094401 (2018).
- [37] P.R. Berman, *Atom Interferometry*, Academic, Chestnut Hill, (1997).
- [38] S. Kleinert, E. Kajari, A. Roura, W.P. Schleich, *Representation-free description of light-pulse atom interferometry including non-inertial effects*, *Phys. Rep.* **605**, 1 (2015).
- [39] M. Cadoret, N. Zahzam, Y. Bidel, C. Diboune, A. Bonnin, F. Théron and A. Bresson, *Phase shift formulation for N-light-pulse atom interferometers: application to inertial sensing*, *J. Opt. Soc. Am. B* **33**, 1777 (2016).
- [40] T. Zanon-Willette, A.V. Taichenachev and V.I. Yudin, *Generalised hyper-Ramsey resonance with spinors*, *Quantum Electron.* **49**, 278 (2019).
- [41] Ch.J. Bordé, Ch. Salomon, S. Avrillier, A. Van Lerberghe, Ch. Bréant, D. Bassi and G. Scoles, *Optical Ramsey fringes with traveling waves*, *Phys. Rev. A* **30**, 1836 (1984).
- [42] Ch. Salomon, *Franges de Ramsey et spectroscopie laser à ultra-haute résolution dans l'infrarouge*, *Phd thesis of Laboratoire de Physique des Lasers, université Paris Nord-Paris XIII.* (1984).
- [43] Ch.J. Bordé, *Density matrix equations and diagrams for high resolution non-linear laser spectroscopy. Application to Ramsey fringes in the optical domain*, in *Advances in Laser Spectroscopy*, edited by H. Walther, F. Strumia and T. Arrecchi, Plenum Press 1983, (1983).
- [44] J. Schwinger, *The Majorana formula*, *Transactions of the New York Academy of Sciences* **38**, 170 (1977).
- [45] M. Hardy, *On Tangents and Secants of Infinite Sums*, *Amer. Math. Monthly.* **123**, 701 (2017).
- [46] M. Born, E. Wolf, *Principles of optics: electromagnetic theory of propagation, interference and diffraction of light*, 7th edition, Cambridge University Press, 1999.
- [47] N. Huntemann, C. Sanner, B. Lipphardt, Chr. Tamm and E. Peik, *Single-Ion Atomic Clock with  $3 \times 10^{-18}$  Systematic Uncertainty*, *Phys. Rev. Lett.* **116**, 063001 (2016).

- [48] C. Sanner, N. Huntemann, R. Lange, Ch. Tamm, E. Peik, M.S. Safronova and S.G. Porsev, *Optical clock comparison for Lorentz symmetry testing*, [\*Nature\* \*\*567\*\*, 204 \(2019\)](#).
- [49] S.M. Brewer, J.-S. Chen, A.M. Hankin, E.R. Clements, C.W. Chou, D.J. Wineland, D.B. Hume and D.R. Leibbrandt, *An  $^{27}\text{Al}^+$  Quantum-Logic Clock with a Systematic Uncertainty below  $10^{-18}$* , [\*Phys. Rev. Lett.\* \*\*123\*\*, 033201 \(2019\)](#).
- [50] By applying a direct transformation to the last pulse  $\tilde{\vartheta}'_p$  of  ${}^qC_{ge}$  as following:
- $$\begin{aligned}\cos \tilde{\vartheta}'_p &\mapsto -i \sin \tilde{\vartheta}'_p e^{-i(\phi'_p + \varphi'_p)} \\ \sin \tilde{\vartheta}'_p &\mapsto i \cos \tilde{\vartheta}'_p e^{-i(\phi'_p + \varphi'_p)}\end{aligned}\quad (53)$$
- we directly get the complex component  ${}^qC_{ge}$  of the composite wavefunction.
- [51] K. Bely, *Hyper-Ramsey spectroscopy with probe-laser-intensity fluctuations*, [\*Phys. Rev. A\* \*\*97\*\*, 031406\(R\) \(2018\)](#).
- [52] I. Ushijima, M. Takamoto and H. Katori, *Operational Magic Intensity for Sr Optical Lattice Clocks*, [\*Phys. Rev. Lett.\* \*\*121\*\*, 263202 \(2018\)](#).
- [53] T. Zanon-Willette, E. de Clercq, and E. Arimondo, *Probe light-shift elimination in generalized hyper-Ramsey quantum clocks*, [\*Phys. Rev. A\* \*\*93\*\*, 042506 \(2016\)](#).
- [54] S.N. Kuznetsov, A.V. Taichenachev, V.I. Yudin, N. Hunteman, K. Sanner, K. Tamm and E. Peik, *Effect of trapped-ion heating on generalised Ramsey methods for suppressing frequency shifts caused by a probe field in atomic clocks*, [\*Quantum Electron.\* \*\*49\*\*, 429 \(2019\)](#).
- [55] K.A. Barantsev, T. Zanon-Willette and A.N. Litvinov, *Generalized Hyper-Ramsey spectroscopy of two-level atoms in an optically dense medium*, [\*Quantum Electron.\* \*\*50\*\*, 934 \(2020\)](#).
- [56] M.H. Levitt, *Symmetry in the design of NMR multiple-pulse sequences*, [\*J. Chem. Phys.\* \*\*128\*\*, 052205 \(2008\)](#).
- [57] Y. Lin, J.P. Gaebler, F. Reiter, T.R. Tan, R. Bowler, Y. Wan, A. Keith, E. Knill, S. Glancy, K. Coakley, A.S. Sørensen, D. Leibfried and D.J. Wineland, *Preparation of Entangled States through Hilbert Space Engineering*, [\*Phys. Rev. Lett.\* \*\*117\*\*, 140502 \(2016\)](#).
- [58] S. Abend, M. Gersemann, C. Schubert, D. Schlippert, E.M. Rasel, M. Zimmermann, M.A. Efremov, A. Roura, F.A. Narducci and W.P. Schleich, *Atom interferometry and its applications*, *Proceedings of the International School of Physics "Enrico Fermi" Course 197 "Foundations of Quantum Theory"*, edited by Ernst M. Rasel, Wolfgang P. Schleich, and Sabine Wölk (IOS, Amsterdam; SIF, Bologna), 345 (2019).
- [59] E. Giese, A.Friedrich, S. Abend, E.M. Rasel and W.P. Schleich, *Light shifts in atomic Bragg diffraction*, [\*Phys. Rev. A\* \*\*94\*\*, 063619 \(2016\)](#).
- [60] S.S. Szigeti, J.E. Debs, J.J. Hope, N.P. Robins and J.D. Close, *Why momentum width matters for atom interferometry with Bragg pulses*, [\*New J. Phys.\* \*\*14\*\*, 023009 \(2012\)](#).
- [61] T. Zanon-Willette, S. Almonacil, E. de Clercq, A.D. Ludlow and E. Arimondo, *Quantum engineering of atomic phase shifts in optical clocks*, [\*Phys. Rev. A\* \*\*90\*\*, 053427 \(2014\)](#).
- [62] K. Moler, D.S. Weiss, M. Kasevich and S. Chu, *Theoretical analysis of velocity-selective Raman transitions*, [\*Phys. Rev. A\* \*\*45\*\*, 342 \(1992\)](#).
- [63] A. Louchet-Chauvet, T. Farah, Q. Bodart, A. Clairon, A. Landragin, S. Merlet and F. Pereira Dos Santos, *The influence of transverse motion within an atomic gravimeter*, [\*New J. Phys.\* \*\*13\*\*, 065025 \(2011\)](#).
- [64] P. Gillot, B. Cheng, S. Merlet and F. Pereira Dos Santos, *Limits to the symmetry of a Mach-Zehnder-type atom interferometer*, [\*Phys. Rev. A\* \*\*93\*\*, 013609 \(2016\)](#).
- [65] L. Morel, Z. Yao, P. Cladé and S. Guellati-Khélifa, *Velocity-dependent phase shift in a light-pulse atom interferometer*, [\*arXiv:2006.14354\* \(2020\)](#).
- [66] M. Cadoret, E. De Mirandes, P. Cladé, F. Nez, L. Julien, F. Biraben and S. Guellati-Khélifa, *Atom interferometry based on light pulses: application to the high precision measurement of the ratio  $h/m$  and the determination of the fine structure constant*, [\*Eur. Phys. J. Spec. Top.\* \*\*172\*\*, 121 \(2009\)](#).
- [67] P. Berg, S. Abend, G. Tackmann, C. Schubert, E. Giese, W.P. Schleich, F.A. Narducci, W. Ertmer and E.M. Rasel, *Composite-light-pulse technique for high-precision atom interferometry*, [\*Phys. Rev. Lett.\* \*\*114\*\*, 063002 \(2015\)](#).
- [68] D. Savoie, M. Altorio, B. Fang, L.A. Sidorenkov, R. Geiger and A. Landragin, *Interleaved atom interferometry for high-sensitivity inertial measurements*, [\*Sci. Adv.\* \*\*4\*\*, eaau7948 \(2018\)](#).
- [69] M. Braun and S.J. Glaser, *Concurrently optimized cooperative pulses in robust quantum control: application to broadband Ramsey-type pulse sequence elements*, [\*New J. Phys.\* \*\*16\*\*, 115002 \(2014\)](#).
- [70] S. Bade, L. Djadaojee, M. Andia, P. Cladé and S. Guellati-Khélifa, *Observation of Extra Photon Recoil in a Distorted Optical Field*, [\*Phys. Rev. Lett.\* \*\*121\*\*, 073603, \(2018\)](#).
- [71] R.H. Parker, C. Yu, B. Esty, W. Zhong, E. Huang and H. Müller, *Controlling the multiport nature of the Bragg diffraction in atom interferometry*, [\*Phys. Rev. A\* \*\*94\*\*, 053618, \(2016\)](#).
- [72] A. Trimeche, M. Langlois, S. Merlet and F. Pereira Dos Santos, *Active Control of Laser Wavefronts in Atom Interferometers*, [\*Phys. Rev. Applied.\* \*\*7\*\*, 034016 \(2017\)](#).
- [73] R. Karcher, A. Imanaliev, S. Merlet and F. Pereira Dos Santos, *Improving the accuracy of atom interferometers with ultracold sources*, [\*New J. Phys.\* \*\*20\*\*, 113041 \(2018\)](#).
- [74] T. Kovachy, J.M. Hogan, A. Sugarbaker, S.M. Dickerson, C.A. Donnelly, C. Overstreet and M.A. Kasevich, *Matter Wave Lensing to Picokelvin Temperatures*, [\*Phys. Rev. Lett.\* \*\*114\*\*, 143004 \(2015\)](#).
- [75] L. Hu, N. Poli, L. Salvi and G.M. Tino, *Atom Interferometry with the Sr Optical Clock Transition*, [\*Phys. Rev. Lett.\* \*\*119\*\*, 263601 \(2017\)](#).
- [76] L. Hu, E. Wang, L. Salvi, J.N. Tinsley, G.M. Tino and N. Poli, *Sr atom interferometry with the optical clock transition as a gravimeter and a gravity gradiometer*, [\*Class. Quantum Grav.\* \*\*37\*\*, 014001 \(2020\)](#).
- [77] M. Abe *et al.*, *Matter-wave Atomic Gradiometer Interferometric Sensor (MAGIS-100)*, [\*arXiv:2104.02835v1\* \(2021\)](#).
- [78] A.V. Taichenachev, V.I. Yudin, C.W. Oates, C.W. Hoyt, Z.W. Barber, and L. Hollberg, *Magnetic Field-Induced Spectroscopy of Forbidden Optical Transitions with Application to Lattice-Based Optical Atomic*

- Clocks*, *Phys. Rev. Lett.* **96**, 083001 (2006).
- [79] Z.W. Barber, C.W. Hoyt, C.W. Oates, L. Hollberg, A.V. Taichenachev, and V.I. Yudin, *Direct Excitation of the Forbidden Clock Transition in Neutral  $^{174}\text{Yb}$  Atoms Confined to an Optical Lattice*, *Phys. Rev. Lett.* **96**, 083002 (2006).
  - [80] X. Baillard, M. Fouché, R. Le Targat, P.G. Westergaard, A. Lecallier, Y. Le Coq, G.D. Rovera, S. Bize and P. Lemonde, *Accuracy evaluation of an optical lattice clock with bosonic atoms*, *Opt. Lett.* **32**, 1812 (2007).
  - [81] A.P. Kulosa, D. Fim, K.H. Zipfel, S. Rühmann, S. Sauer, N. Jha, K. Gibble, W. Ertmer, E.M. Rasel, M.S. Safronova, U.I. Safronova and S.G. Porsev, *Towards a Mg Lattice Clock: Observation of the  $^1S_0 - ^3P_0$  Transition and Determination of the Magic Wavelength*, *Phys. Rev. Lett.* **115**, 240801 (2015).
  - [82] T. Akatsuka, M. Takamoto and H. Katori, *Optical lattice clocks with non-interacting bosons and fermions*, *Nature Phys* **4**, 954 (2008).
  - [83] R. Hobson, W. Bowden, S.A. King, P.E.G. Baird, I.R. Hill and P. Gill, *Modified hyper-Ramsey methods for the elimination of probe shifts in optical clocks*, *Phys. Rev. A* **93**, 010501(R) (2016).
  - [84] Ch. Sanner, N. Huntemann, R. Lange, Ch. Tamm and E. Peik, *Autobalanced Ramsey Spectroscopy*, *Phys. Rev. Lett.* **120**, 053602 (2018).
  - [85] V.I. Yudin, A.V. Taichenachev, M. Yu. Basalaev, T. Zanon-Willette, J.W. Pollock, M. Shuker, E.A. Donley and J. Kitching, *Generalized Autobalanced Ramsey Spectroscopy of Clock Transitions*, *Phys. Rev. Applied* **9**, 054034 (2018).
  - [86] K. Bongs, M. Holynski, J. Vovrosh, P. Bouyer, G. Condon, E. Rasel, C. Schubert, W.P. Schleich and A. Roura, *Taking atom interferometric quantum sensors from the laboratory to real-world applications*, *Nat Rev Phys* **1**, 731 (2019).
  - [87] J. Grotti, S. Koller, S. Vogt, S. Vogt, S. Haßner, U. Sterr, C. Lisdat, H. Denker, C. Voigt, L. Timmen, A. Rolland, F.N. Baynes, H.S. Margolis, M. Zampalo, P. Thoumany, M. Pizzocaro, B. Rauf, F. Bregolin, A. Tampellini, P. Barbieri, M. Zucco, G.A. Costanzo, C. Clivati, F. Levi and D. Calonico, *Geodesy and metrology with a transportable optical clock*, *Nature Phys* **14**, 437 (2018).
  - [88] M. Delahaye and C. Lacroûte, *Single-ion, transportable optical atomic clocks*, *Journal of Modern Optics*, **65**, 622 (2018).
  - [89] X. Wu, Z. Pagel, B.S. Malek, T.H. Nguyen, F. Zi, D.S. Scheirer and H. Müller, *Gravity surveys using a mobile atom interferometer*, *Sci. Adv.* **5**, eaax0800 (2019).
  - [90] Y. Bidel, N. Zahzam, C. Blanchard, A. Bonnin, M. Cadoret, A. Bresson, D. Rouxel and M.F. Lequentrec-Lalancette, *Absolute marine gravimetry with matter-wave interferometry*, *Nat. Commun.* **9**, 627 (2018).
  - [91] V. Ménoret, P. Vermeulen, N. Le Moigne, S. Bonvalot, P. Bouyer, A. Landragin and B. Desruelle, *Gravity measurements below  $10^{-9}g$  with a transportable absolute quantum gravimeter*, *Sci. Rep.* **8**, 12300 (2018).
  - [92] O. Hosten, N.J. Engelsen, R. Krishnakumar and M.A. Kasevich, *Measurement noise 100 times lower than the quantum-projection limit using entangled atoms*, *Nature*, **505** (2016).
  - [93] L. Salvi, N. Poli, V. Vuletić and G.M. Tino, *Squeezing on Momentum States for Atom Interferometry*, *Phys. Rev. Lett.* **120**, 033601 (2018).
  - [94] C. Brif, B.P. Ruzic, and G.W. Biedermann, *Characterization of Errors in Interferometry with Entangled Atoms*, *PRX Quantum* **1**, 010306, (2020).
  - [95] H. Abele, T. Jenke, H. Leeb, and J. Schmiedmayer, *Ramsey's method of separated oscillating fields and its application to gravitationally induced quantum phase shifts*, *Phys. Rev. D* **81**, 065019 (2010).
  - [96] J.M. Hogan *et al.*, *An atomic gravitational wave interferometric sensor in low earth orbit (AGIS-LEO)*, *Gen. Relativ. Gravit.* **43**, 1953 (2011).
  - [97] P.W. Graham, J.M. Hogan, M.A. Kasevich and S. Rajendran, *New Method for Gravitational Wave Detection with Atomic Sensors*, *Phys. Rev. Lett.* **110**, 171102 (2013).
  - [98] S. Kolkowitz, I. Pikovski, N. Langellier, M.D. Lukin, R.L. Walsworth and J. Ye, *Gravitational wave detection with optical lattice atomic clocks*, *Phys. Rev. D* **94**, 124043 (2016).
  - [99] B. Canuel *et al.*, *Exploring gravity with the MIGA large scale atom interferometer*, *Sci. Rep.* **8**, 14064 (2018).
  - [100] M.S. Safronova, D. Budker, D. DeMille, D.F. Jackson Kimball, A. Derevianko and C.W. Clark, *Search for new physics with atoms and molecules*, *Rev. Mod. Phys.* **90** 025008 (2018).